NASA-CR-195769

FINAL
IN-25-CR
11761
P. 43

MODELLING DIRECTIONAL SOLIDIFICATION

Final Report on Grant NAG8-831

1 May 1991 to 31 May 1994

CLARKSON UNIVERSITY

Potsdam, New York 13699-5700

Investigators:

Dr. William R. Wilcox
Dean, School of Engineering
(315) 268-6446; fax 3841
email: WILCOX@AGENT.CLARKSON.EDU

Dr. Liya L. Regel
Director, International Center for Gravity Materials Science and Applications
(315) 268-7672; fax 3841
email: REGEL@AGENT.CLARKSON.EDU

(NASA-CR-195769) MODELLING DIRECTIONAL SOLIDIFICATION Final Report, 1 May 1991 - 31 May 1994 (Clarkson Univ.) 43 p

N94-34684

Unclas

G3/25 0011761

S U M M A R Y

Goal and Objective

This grant, NAG8-831, was a continuation of a previous grant, NAG8-541. The long range goal of this program has been to develop an improved understanding of phenomena of importance to directional solidification, in order to enable explanation and prediction of differences in behavior between solidification on Earth and in space. Emphasis in the recently completed grant was on determining the influence of perturbations on directional solidification of InSb and InSb-GaSb alloys. In particular, the objective was to determine the influence of spin-up/spin-down (ACRT), electric current pulses and vibrations on compositional homogeneity and grain size.

Results

1. Six papers were published, two PhD dissertations completed, research for another PhD dissertation nearing completion, one MS thesis completed, and sixteen talks and papers presented. These are listed at the end of this summary.

2. Developed techniques for interface demarcation of InSb-GaSb alloy and doped InSb [D1, D2, D3].

3. Using interface demarcation, showed that the freezing rate did not equal the ampoule lowering rate and varied significantly throughout each run in our Bridgman-Stockbarger equipment [D1, D3].

4. The axial composition profile in InSb-GaSb always corresponded to complete mixing in the melt with equilibrium at the freezing interface. No cross sectional variations in composition were observed. These results were obtained without stirring, with ACRT, with vibration, and with application of current pulses unless interface breakdown occurred [D1, D2].

5. Temperature variations in the melt following application and cessation of electric current corresponded to expectations from theory [D1].

6. Developed etching techniques to clearly reveal and distinguish grain and twin boundaries by development of grooves along these boundaries [D3].

7. Periodic application of a large electric current pulses during directional solidification of InSb-GaSb alloy caused a finer grain structure, compositional fluctuations, and many cracks [D1].

8. Application of axial vibrations during directional solidification of InSb-GaSb alloy led to much larger grains and slightly increased twinning [D1, D4]. The interface curvature during the first half of the ingots was not influenced by vibration, but became slightly more concave during the second half. Vibration decreased the freezing rate slightly.

9. Vibration greatly decreased the initial freezing rate of InSb and greatly increased the grain size at the beginning of the ingot [4]. Vibration was particularly effective in increasing grain size for larger diameter ingots.

10. Vibration reduced the axial variation in electrical resistivity of Te-doped InSb and InSb-GaSb alloys [4].

11. Vibration increased the heat transfer coefficient between the molten charge and the furnace [4],

12. The grain size in InSb-GaSb and in InSb depended on rotation rate in the Accelerated Crucible Rotation Technique (ACRT, or spin-up/spin-down) [D2, D4]. There appeared to be an optimal rotation rate, but reproducibility was poor. ACRT caused the InSb-GaSb interface shape to become slightly less concave and the InSb to become more concave. ACRT was more effective at increasing the grain size for larger diameter InSb.

13. Striations were produced in Te-doped InSb by pulses of electric current and by ACRT [D3]. These striations tended to change direction at grain and twin boundaries, indicating that the freezing interface did not correspond to an isotherm.

14. Striations were produced in Te-doped InSb solidified by rotation during ACRT [D3, P4].

15. Using current interface demarcation with InSb, we showed that melt-back occurred when ampoule rotation was turned off and when it was turned on [D3, P4]. ACRT caused the freezing rate to vary. The net amount of material solidified while the ampoule was rotated differed from that solidified with rotation off, although the time intervals were identical and the ampoule translation rate was constant. These results were in agreement with our earlier mass transfer measurements [P1].

16. Vibration during solidification increased the lamellar spacing and decreased the grain size of lead-tin eutectic [P5, P6].

17. The furnace temperature profile had a strong influence on buoyancy-driven convection and doping homogeneity [P3].

PhD Dissertations and MS Thesis

D1. Mohsen Banan, "Influence of Imposed Perturbations on Directional Solidification of $In_xGa_{1-x}Sb$ Alloy Semiconductor," PhD Dissertation, Clarkson University (1991).

D2. Ross T. Gray, "Influence of the Accelerated Crucible Rotation Technique on the Directional Solidification of InSb-GaSb Alloys," PhD Dissertation, Clarkson University (1991).

D3. Jian Zhou, "Accelerated Crucible Rotation Technique and Current Interface Demarcation during Directional Solidification of Te-Doped InSb," MS Thesis, Clarkson University (1992).

D4. Weijun Yuan, PhD research in progress.

Publications

P1. M. Larrousse and W.R. Wilcox, "Interfacial Mass Transfer to a Cylinder Endwall During Spin-up/Spin-down," Chem. Eng. Sci. 45, 1571-1581 (1990).

P2. M. Banan, R.T. Gray and W.R. Wilcox, "An Experimental Approach to Determine the Heat Transfer Coefficient in Directional Solidification Furnaces," J. Crystal Growth 113, 557-565 (1991).

P3. G.T. Neugebauer and W.R. Wilcox, "Experimental Observation of the Influence of Furnace Temperature Profile on Convection and Segregation in the Vertical Bridgman Crystal Growth Technique," Acta Astronautica 25, 357-362 (1991).

P4. J. Zhou, M. Larrousse, W.R. Wilcox and L.L. Regel, "Directional Solidification with ACRT," J. Crystal Growth 128, 173-177 (1993).

P5. R. Caram, M. Banan and W.R. Wilcox, "Directional Solidification of Pb-Sn Eutectic with Vibration," J. Crystal Growth 114, 249-254 (1991).

P6. R. Caram, M. Banan and W.R. Wilcox, "Effect of Vibration on Unidirectional Growth of Lead-Tin Eutectic Alloy," Congr. Anu. - Assoc. Bras. Met., 46th, 301-18 (1991).

Talks and Papers Presented

T1. W.R. Wilcox, "Transport Phenomena in Directional Solidification," Tufts University (March 1990).

T2. M. Banan, R. Gray and W.R. Wilcox, "Directional Solidification of InGaSb," Gordon Research Conference on Crystal Growth, Ventura (March 1990).

T3. W.R. Wilcox, "Influence of Low Gravity, Magnetic Field, Vibrations, Current Pulses and Accelerated Crucible Rotation on Directional Solidification of Indium Gallium Antimonide," LIMSI, Orsay (April 1990).

T4. M. Banan, R.T. Gray and W.R. Wilcox, "GaSb-InSb Alloy Growth," CSME, Toronto (June 1990).

T5. M. Banan, R. Gray and W.R. Wilcox, "Solidification and Characterization of Indium Gallium Antimonide," Northeast Regional Meeting (NERM) of the American Chemical Society, Potsdam, NY (June 1990).

T6. M. Banan and W.R. Wilcox, "Effect of Axial Oscillation of the Growth Ampoule on Solidification of $In_xGa_{1-x}Sb$," Eighth American Conference on Crystal Growth (ACCG-8), Vail (July 1990).

T7. R.T. Gray and W.R. Wilcox, "Influence of ACRT on Directional Solidification of InSb-GaSb Alloys," ACCG-8 (July 1990).

T8. W.R. Wilcox, "Crystallization of $In_xGa_{1-x}Sb$," Ioffe Physico-Technical Institute, Leningrad, USSR (August 1990).

T9. G.T. Neugebauer and W.R. Wilcox, "Experimental Observation of the Influence of Furnace Temperature Profile on Convection and Segregation in the Vertical Bridgman Crystal Growth Technique," IAF, Dresden (October 1990).

T10. J. Zhou, M. Banan, R. Gray and W.R. Wilcox, "Use of Current Interface Demarcation During Directional Solidification of Te-Doped InSb with ACRT," Third Canadian Materials Science Conference, Kingston (June 1991).

T11. W.R. Wilcox, "Gravitational Effects on Directional Solidification of Indium Antimonide and Indium Gallium Antimonide," University of Colorado, Boulder (August 1991).

T12. J. Zhou, M. Banan, R. Gray and W.R. Wilcox, "ACRT Striations and the use of Current Interface Demarcation during Directional Solidification of Te-doped InSb," Fourth Eastern Regional Conference on Crystal Growth (ACCG/East-4), Atlantic City (October 1991).

T13. R. Gray, M. Banan, J. Zhou, M. Larrousse and W.R. Wilcox, "Influence of Perturbations on Directional Solidification of InSb-GaSb Alloy Semiconductors," AIAA, Reno (January 1992).

T14. J. Zhou, M. Larrousse and W.R. Wilcox, "Directional Solidification with ACRT," Tenth International Conference on Crystal Growth (ICCG-10), San Diego (August 1992).

T15. J. Zhou, M. Larrousse and W.R. Wilcox, "Directional Solidification with ACRT," ICCG-10 (August 1992).

T16. W.J. Yuan, M. Banan, L.L. Regel and W.R. Wilcox, "Directional solidification of InSb-GaSb Alloy with Vibration of the Ampoule," International Workshop on g-Jitter (June 1993).

INFLUENCE OF FURNACE TEMPERATURE PROFILE ON BUOYANCY-DRIVEN CONVECTION

Azulene-doped naphthalene was directionally solidified by the vertical Bridgman-Stockbarger technique [P3]. Doping inhomogeneity and convection were determined as a function of the temperature profile in the furnace and the freezing rate. The convection velocity was two orders of magnitude lower when the temperature increased with height than when it decreased with height. Rarely was the convection pattern axisymmetric, even though the temperature varied less than 0.1 K around the circumference of the growth ampoule. Correspondingly, the cross-sectional variation in azulene concentration tended to be asymmetric, especially when the temperature increased with height. This cross-sectional variation changed dramatically along the ingot, reflecting changes in convection, presumably due to the decreasing height of the melt.

Although there was large scatter and irreproducibility in the cross-sectional variation in doping, this variation tended to be least when the growth rate was low and the convection was vigorous. It is expected that compositional variations would also be small at high growth rates with weak convection and a flat interface. Neither slow rotation of the ampoule nor deliberate introduction of thermal asymmetry during solidification had a significant influence on the magnitude of the cross-sectional variation in doping.

It was predicted that slow directional solidification under microgravity conditions could produce greater inhomogeneities than on Earth.

INFLUENCE OF SPIN-UP/SPIN-DOWN (ACRT)

We performed several studies on the application of the accelerated crucible rotation technique (ACRT) to vertical Bridgman crystal growth [P1, P4, D2, D3]. In our experiments the ampoule was rotated about its axis at a constant velocity. The ampoule was alternately rotated and stationary for equal time periods.

In our first set of experiments, the electrochemical limiting current density technique was used to measure the local rate of mass transfer to the bottom endwall of a large aspect ratio cylinder [P1, P4]. Flow visualization experiments were also performed using photography of the motion of suspended particles. The local mass transfer rate was a strong function of radial position. At the center during spin-up from rest, the maximum enhancement in mass transfer occurred after the Ekman time scale and before the viscous time scale. At the center during spin-down to rest, a stagnation vortex formed, causing the mass transfer rate to decay and then increase back to the original value on the order of the viscous time scale. Away from the center, a much more complicated pattern was observed, but spin-up and spin-down were similar. Two maxima in mass transfer rate occurred for an Ekman number over 0.0074. Alternating spin-up and spin-down with a short period caused the center of the endwall to experience a nearly sinusoidal variation in mass transfer, with the frequency equal to the forcing frequency. Near the edge, the frequency was twice the forcing frequency.

In our second set of experiments, $In_{0.2}Ga_{0.8}Sb$ was solidified with and without ACRT for various rates and periods [D2]. No significant radial segregation was found in any ingot, either with or without ACRT. The axial composition profiles all corresponded to the well-mixed condition. Application of ACRT with a rotation rate of 80 rpm consistently led to the fewest grain and twin boundaries, i.e. the largest grain size. Interface demarcation studies revealed that application of ACRT with a rotation rate of 80 rpm led to a reduction in interface depth from 0.6 mm to 0.3 mm. We believe that this less concave interface was responsible for the larger grain size.

In the third set of experiments, Te-doped InSb was solidified with and without ACRT and current interface demarcation (CID) [P4, D3]. Etching revealed both current and ACRT-induced striations. These striations changed direction when they crossed twin or grain boundaries. The striations showed that ACRT had a negligible effect on the interface shape, although the interface position was shifted during each ACRT cycle, causing a periodic variation in the growth rate. Some of the current pulses produced no striations during ACRT, suggesting that backmelting occurred during spin-up.

For the current, fourth set, of ACRT experiments, Yuan [4] is using periodic rotation of the growth ampoule with 40-120 rpm and 20

seconds rotation on and 20 seconds rotation. InSb ingots were directionally solidified in a VBS furnace at 8 mm/hr and 20°C/cm axial temperature gradient. The current interface demarcation technique [D3] was used to measure the growth rate. The ingot grown with 80 rpm ACRT with 20 seconds rotation on and 20 seconds rotation off had fewer grains than ingots grown without ACRT. The interface shape was concave when ACRT was applied. Resistivity was measured by a 4-point probe on wafers made from the 22 mm diameter InSb ingots. There was some axial variation in resistivity. ACRT made the variation smaller. No significant radial variations were observed.

INFLUENCE OF ELECTRIC CURRENT PULSES

$In_{0.2}Ga_{0.8}Sb$ was solidified with and without periodic application of large electric current pulses, so as to give a varying freezing rate [D1]. In the regions solidified with periodic application of current, the microstructure consisted of fine grains and microcracks and there were significant axial and radial composition fluctuations. The fine grain structure and composition fluctuations are attributed to interface breakdown caused by the increase in growth rate when Peltier cooling was taking place.

Current interface demarcation during solidification of Te-doped $In_{0.2}Ga_{0.8}Sb$ showed irregularities at grain boundaries and a slight shift across twin boundaries, similar to that reported above for Te-doped InSb.

Periodic passage of 15.7 amp/cm^2 through $In_{0.2}Ga_{0.8}Sb$ for 60 s followed by no current caused a sinusoidal temperature variation of 1.5 K.

INFLUENCE OF VERTICAL VIBRATION

$In_{0.2}Ga_{0.8}Sb$ was solidified with and without low frequency axial vibration [D1]. The axial composition profile always corresponded to perfect mixing of the melt. The composition was uniform in cross sections, unless the growth rate were large enough to cause interface breakdown due to constitutional supercooling. There appeared to be fewer grain boundaries, more twin boundaries, and a more convex interface shape with vibration. During vibration, twins mostly began at the ampoule wall.

Axial vibration increased the lamellar spacing and decreased the grain size of lead-tin eutectic [D1, P5, P6].

The current work by Yuan [4] has involved solidification of $In_{0.2}Ga_{0.8}Sb$ and InSb in a vertical Bridgman-Stockbarger apparatus with axial vibration of the growth ampoule at a frequency of 10-100

Hz and an amplitude of 0.01-0.5 mm amplitude. The ampoule travel rate was 8 mm/day and the axial temperature gradient was 30-35°C/cm. Energy dispersive X-ray spectrometry has been used for compositional analysis of the ingots. Optical microscopy has been used for the examination of the microstructure of the ingots. The quenched interface demarcation technique [D2] has been used to reveal the solid/melt interface shape and determine the average growth rate.

The average growth rate of $In_{0.2}Ga_{0.8}Sb$ decreased with the progress of the solidification. The average growth was greater than the ampoule translation rate during solidification of the first half of the ingot, and lower than the ampoule translation rate during the second half. Vibration did not change the average growth rate very much. For example, with a 20 Hz frequency and 0.5 mm amplitude vibration, the average growth rate decreased slightly during the last-to-freeze part of the ingot.

Vibration caused no noticeable change in the solid/melt interface shape during solidification of the first half of $In_{0.2}Ga_{0.8}Sb$ ingots. Vibration made the interface more concave during solidification of the second half.

Both with and without vibration of the growth ampoule, the axial compositional profiles of the InSb-GaSb corresponded to a well-mixed melt. There was no significant radial compositional variation. However, there was a wave-like radial compositional profile near the end of the ingot, whether vibration was applied or not.

The $In_{0.2}Ga_{0.8}Sb$ ingots grown with vibration had fewer grains and more twins than those grown without vibration, especially at the first-to-freeze part of the ingots. The ingots grown with 20 Hz frequency and 0.5 mm amplitude had the fewest grains.

InSb also has been directionally solidified in a VBS furnace, at 8 mm/hr and 20°C/cm axial temperature gradient. Current interface demarcation technique has been used to measure the growth rate. Without vibration, the growth rate was very high initially. It decreased very rapidly to a steady-state value, which was higher than the ampoule translation rate. Application of vibration decreased the growth rate, especially at the first-to-freeze end of the ingots. With vibration, the initial growth rate was lower than the ampoule translation rate. Then the growth rate increased with the progress of solidification. During solidification of the second half of the ingot, the growth rate was approximately equal to the ampoule translation rate.

Application of vertical vibration decreased the number of curved boundaries in InSb, especially at the first-to-freeze part of the ingots. However, the number of straight boundaries was increased.

Application of vibration greatly improved the grain size for large diameter InSb ingots.

Resistivity was measured using a 4-point probe on wafers made from 22 mm diameter InSb ingots. There was some axial variation in resistivity. Vibration decreased this variation. No significant radial variation was observed.

The temperature in the melt was measured with an immersed thermocouple. This temperature increased right after the vibration was turned on. After about 2 minutes, the temperature decreased to its value before the vibration was turned on. Temperature increases were observed both near the solid/liquid interface and far away from interface. The heat translation coefficient between the charge and the furnace was evaluated experimentally by our lumped transient analysis technique [P2]. The heat transfer coefficient increased by 30% when 20 Hz frequency/0.5 mm amplitude vibration was applied.

CURRENT EXPERIMENTS

Figure 1 shows the experimental setup for solidification of InSb-GaSb and InSb. With this apparatus, the growth ampoule could be vibrated or rotated. Table 1 shows the solidification conditions for the experiments. The axial furnace temperature profiles for these conditions are shown in figures 2 and 3.

The starting growth materials were 6N purity In, Ga and Sb. Elemental shots were weighed and sealed in a pre-cleaned ampoule under a vacuum of 10^{-6} torr. Before the growth, the material was pre-alloyed in our rocking furnace at 800°C overnight. In some experiments, 6N purity Te was added to the growth materials as a dopant. The dopant concentration was about 1 10^{20} atoms/cm^3.

The quenched interface technique [D2] was used to reveal the interface shape for solidification of InSb-GaSb. Figure 4 shows the schedule for demarcation experiments. The average growth rate was calculated from the experiments. The same schedule was used for solidification of InSb with ACRT. Current interface demarcation was used with growth of InSb. A 10 A DC current pulse with 0.05 seconds duration was passed through the charge with positive at melt and negative at solid. The growth rate was calculated from CID experiment for solidification of InSb.

The microstructure of the ingots was examined by using optical microscopy. Many efforts were used to distinguish curved twin boundaries from grain boundaries according to the clues in Gray's work [D2]. The number of boundaries was counted every 2 mm along the growth direction.

SEM-EDS was used to measure the compositional profiles for InSb-GaSb ingots. A least-squares analysis was used to calculate the mole fraction of InSb in the unknown sample. Resistivity was measured for the 22 mm diameter InSb ingots using a VP-10e 4-point resistivity tester. Both axial and radial profiles were measured.

Figure 5 shows the ampoule for temperature measurement experiments. The ampoule was charged with InSb. The temperature was measured and recorded by a Z-248 computer through a data acquisition system. Temperature set points in the hot zone and cold zone of the furnace were the same as those in the growth experiments.

The effect of vibration on directional solidification of InSb-GaSb

Figure 6 shows the axial compositional profiles for InSb-GaSb ingots. Vertical vibration of the ampoule didn't change the axial compositional profile. All of the axial compositional profiles corresponded to a well-mixed melt, for ingots grown with and without vibration. Figure 7 shows the radial compositional profiles for InSb-GaSb ingots. No significant radial compositional variation was observed for ingots grown with and without vibration. Near the end of the ingot, there was a wave-like radial compositional variation.

Figure 8 shows the average growth rate, determined by dividing the distance between every pair of striations by the time interval between generation of these two demarcations. During the first half of the ingots, the average growth rate was larger than the ampoule translation rate. It decreased with the progress of solidification and became less than the ampoule translation rate during the second half of the ingot. There was a small increase near the end of the solidification for all ingots. Vibration did not noticeably affect the growth rate.

Figure 9 shows the interface depth change from the quenched interface demarcation experiment. Interface depth was defined by the difference between the average location of the interface at the edge of the ingot and the minimum of the interface. For the ingots grown both with and without vibration, the interface depth increased in the second half of the ingots. Vibration did not affect the interface depth during the first half of the ingot. However, vibration made the interface more concave during the second half of the ingot. Near the end of the ingot, the interface became a little concave.

Figure 10 shows the relative interface velocity calculated from the demarcation experiments. When a 20 Hz frequency/0. 5 mm amplitude vibration was applied, the relative interface velocity decreased. When the frequency of vibration was increased to 40 Hz, the relative interface velocity increased to the value without vibration.

The microstructure of InSb-GaSb ingots was quantified by counting and comparing the number of curved and straight boundaries. Figure 11 shows the microstructure of InSb-GaSb ingots grown without and with 20 Hz/0. 5 mm amplitude vibration. Many efforts were made to distinguish grain boundaries from curved twin boundaries. The number of grain boundaries and twin boundaries were counted across the ingots. There were fewer curved boundaries in the ingot grown with vibration but more straight boundaries, as shown in figure 12. The ingots grown with 20 Hz frequency/0.5 mm amplitude had the fewest grain boundaries. Table 2 lists the number of grain boundaries and twin boundaries for InSb-GaSb grown under different conditions.

For the same amplitude, vibration at a different frequency induces a different dynamic acceleration. There were minimum grain boundaries at a dynamic acceleration of 0.18 g, which corresponds to a 20 Hz frequency vibration. Figure 13 shows the effect of dynamic acceleration on the number of boundaries in InSb-GaSb ingots.

Solidification of InSb with vibration

The growth rate was calculated from the CID experiment. Figure 14 shows the growth rate for InSb ingots grown without and with 20 Hz/0.5 mm amplitude vibration. For InSb grown without vibration, at the beginning of the ingot, the growth rate was about 3 times the ampoule translation rate, but it decreased very fast. During the entire growth period, the growth rate was larger than the ampoule translation rate. Near the end of the ingot, the growth rate increased slightly again.

Vibration decreased the growth rate for solidification of InSb. No higher growth rate at the first-to-freeze part was observed. When a 20 Hz frequency/0.5 mm vibration was applied, during the first half part of the ingot, the growth rate was lower than the ampoule translation rate. At the beginning of the ingot, the growth rate was about the half the ampoule translation rate. The growth rate increased with solidification. When about half of the melt was solidified, the growth rate was approximately equal to the ampoule translation rate. No growth rate increase near the end of the ingot was observed.

When the frequency was higher than 50 Hz, the resulting ingot was in pieces.

Ingots solidified with vibration had fewer curved boundaries than ingots grown without vibration, but had more straight boundaries. It was obvious that axial vibration of the ampoule improves the grain size at the beginning of the ingots. Without vibration, there were many fine grains in the first-to-freeze end of the ingot. With vibration, the grain size was increased. Figure 15

shows the microstructure of InSb ingots grown with and without vibration. Some ingots were solidified with vibration periodically applied to the ampoule. Fewer curved boundaries were observed in ingots grown with periodic application of vibration, as shown in figure 16.

Some large diameter InSb ingots were solidified without and with vibration. For an ingot grown with 20 Hz/0.5 mm amplitude vibration, there were a few large grains with some twins. Vibration of the ampoule greatly improved the grain size for large diameter InSb ingots. Figure 17 shows the microstructure for the 22 mm diameter InSb ingots.

Resistivity of the InSb ingots was measured by a 4-point probe resistivity tester. The sample was scanned at 2 mm intervals. The resistivity changed along the growth axis of the ingot for ingots grown without vibration. Vibration made the resistivity more uniform along the growth axis, except for the last-to-freeze part of the ingot, as shown in figure 18. Figure 19 shows the radial resistivity for InSb ingots grown with and without vibration. Radial resistivity did not change very much for ingots grown both with and without vibration.

Temperature changes induced by vibration

The axial temperature profile was measured with an empty ampoule and with an ampoule containing InSb, with and without vibration. An ampoule with 22 mm ID 24 mm OD was used. The temperature profile was measured outside the ampoule wall at the (a) bottom center, (b) 3 cm and (c) 7 cm above the bottom. In case (c), the temperature measurement point was at the top of the charge. The temperature in the molten InSb was measured using a 9 mm ID X 11 mm OD ampoule. The temperature was measured at one point in the melt far away from the interface, and at another near the interface. The temperature was recorded by a Z-248 computer every 0.5 second using a data acquisition system.

Figures 20 - 22 show the temperature profile measured along the outside ampoule wall. When the ampoule contained InSb, the temperature at the bottom of the ampoule was increased. Vibration of the ampoule did not affect the temperature at the bottom of the ampoule. With an InSb charge, the temperature profile of the furnace, when measured 3 cm above the bottom, was higher than with an empty ampoule. Vibration of an ampoule containing InSb caused the temperature in the hot zone to decrease, but did not affect the temperature in the cold zone. However, at the top of the charge, vibrating the ampoule made the temperature decrease.

The temperature in the melt was measured *in situ* when vibration was applied to the growth ampoule. Temperature in the melt increased right after vibration was induced. When vibration had continued

for about 2 minutes, the temperature decreased to the value before vibration. A temperature rise was observed both near the solid/melt interface and far away from the interface, as shown in figures 23 and 24.

The heat transfer coefficient h between the charge and the furnace was evaluated experimentally by using our lumped transient analysis method [P2]. Table 3 shows the heat transfer coefficient determined in these experiments. With an InSb charge, when a 20 Hz frequency/0.5 mm amplitude vibration was applied to the growth ampoule, the heat transfer coefficient h between the charge and the furnace increased about 30%. With a vibration of 60 Hz frequency and 0.05 mm amplitude, the heat transfer coefficient between the charge and the furnace decreased, but it was still larger than without vibration, as shown in figure 25.

Solidification of InSb with rotation of the ampoule

InSb ingots were solidified with periodic rotation of the ampoule (ACRT). The ingot diameter was either 9 mm or 22 mm. A square wave rotation schedule was used; the rotation on time and off time were both 20 seconds. CID was used with ACRT. With some 22 mm diameter ingots, quenched interface demarcation was used. The microstructure was examined, and the resistivity was measured for these ingots. Rotational striations were revealed in some ingots.

For small diameter InSb ingots, the microstructure was mainly small grains. ACRT did not improve the grain size for 9 mm InSb ingots. For large diameter (22 mm) InSb ingots, when 80 rpm ACRT was applied to the growth ampoule with 20 seconds on and 20 seconds off, fewer grains was observed. The grains started from the beginning part of the ingot and extended to the whole ingot. Some twins were present in the bigger grains. Figure 26 shows the microstructure of InSb ingots solidified with and without ACRT.

Rotational striations were observed for InSb grown with 80 rpm ACRT. The solid/melt interface was concave during the whole ingot. The interface became more and more concave with progressive solidification.

The resistivity of the InSb was measured for 22 mm ingots axially and radially. Under different ACRT conditions, the resistivity was uniform axially, except for the first- and last-to-freeze ends of the ingots. Figure 27 and figure 28 shows the resistivity profiles for InSb ingots solidified with ACRT. No significant radial resistivity variation was observed.

Table 1 Conditions for solidification of InSb-GaSb and InSb

Conditions for solidification of InSb-GaSb:		Conditions for solidification of InSb:	
Hot zone temperature:	800 °C	Hot zone temperature:	600 °C
Cold zone temperature:	480 °C	Cold zone temperature:	450 °C
Initial InSb molar fraction:	0.2	Ampoule translation rate:	8 mm/hr.
Ampoule translation rate:	8 mm/day		

Table 2 Number of grain and twin boundaries of InSb-GaSb ingots

Ingot	Vibration	Grain boundaries	Twin boundaries
GA-1	no	1.16±0.42	1.20±0.17
GV-1	20 Hz/0.5 mm	0.37±0.19	1.38±0.14
GV-5	40 Hz/0.1 mm	0.63±0.10	1.47±0.12
GV-6	60 Hz/0.05 mm	0.64±0.14	1.37±0.17
GV-2	100 Hz/0.01 mm	0.67±0.14	1.30±0.19

Table 3 Heat translation coefficient between the charge and furnace

Run No.	Temperature °C				Bi	$h \times 10^2$ (J/cm^2·K·s)
	T_w	T_i	T_∞	T_0		
	no vibration					
1	680	570	652.3	568.9	0.02425	0.998
2	670	570	549.3	644.0	0.02406	0.989
3	670	570	647.9	549.4	0.02370	0.975
4	680	600	592.2	662.4	0.02392	0.984
	20 Hz/0.5 mm vibration					
5	680	596	586.0	659.3	0.03071	1.263
6	680	595	652.9	585 1	0.03027	1.245
7	675	590	570.0	647.3	0.03050	1.255
8	670	570	553.0	647.7	0.02833	1.165
9	670	570	638.8	556.6	0.02901	1.993
10	670	555	549.0	636.1	0.02993	1.231
	60 Hz/0.05 mm vibration					
11	690	575	564.0	643.7	0.02747	1.130
12	680	590	650.3	565.1	0.02690	1.106
13	660	545	543.0	632.9	0.02487	1.023
14	670	560	644.3	547.7	0.02819	1.159

Figure 1 Experimental setup

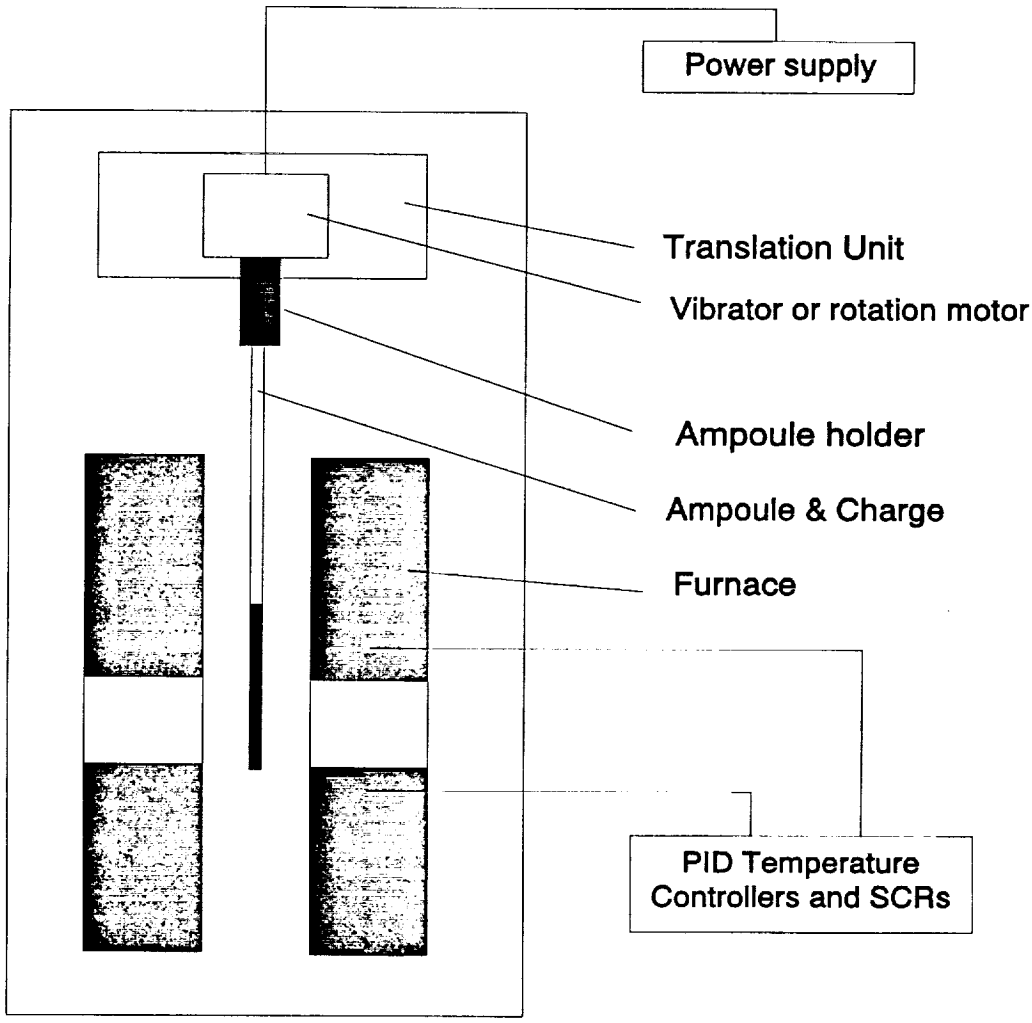

Figure 2 Temperature profiles for solidification of InSb-GaSb

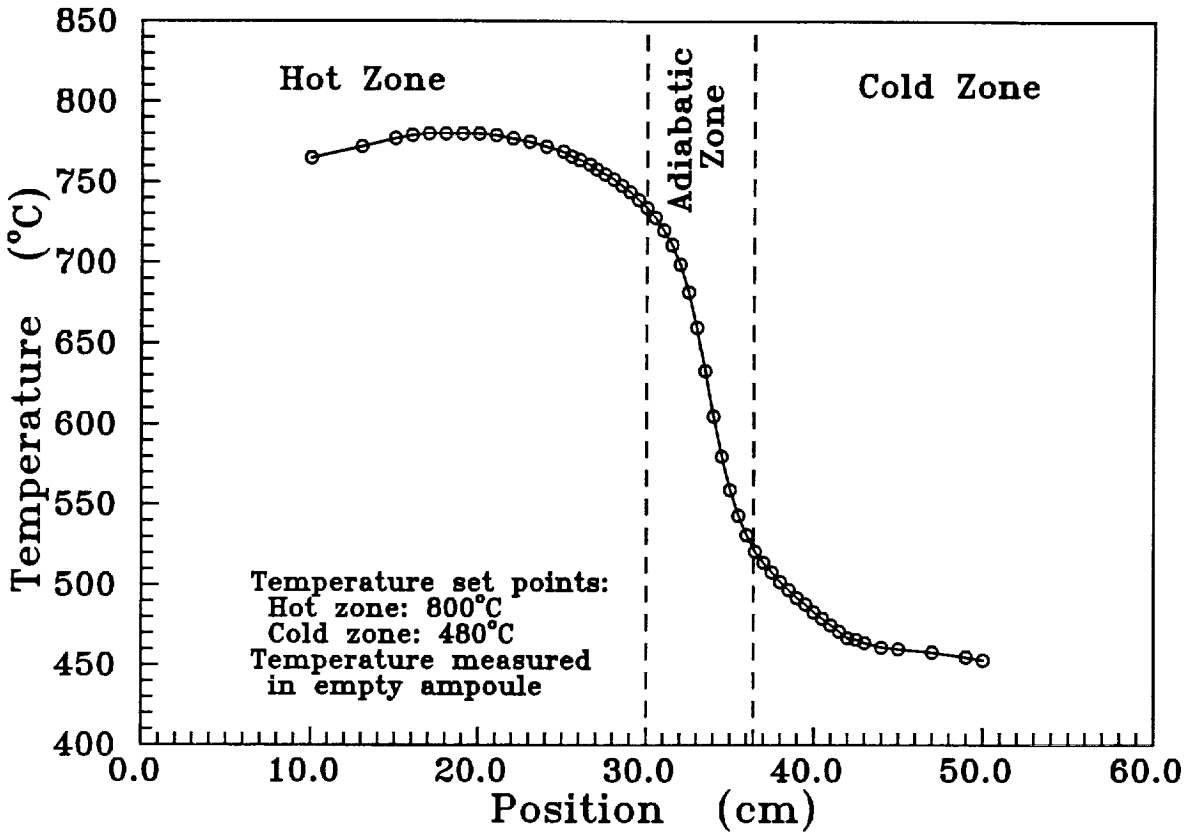

Figure 3 Temperature profiles for solidification of InSb

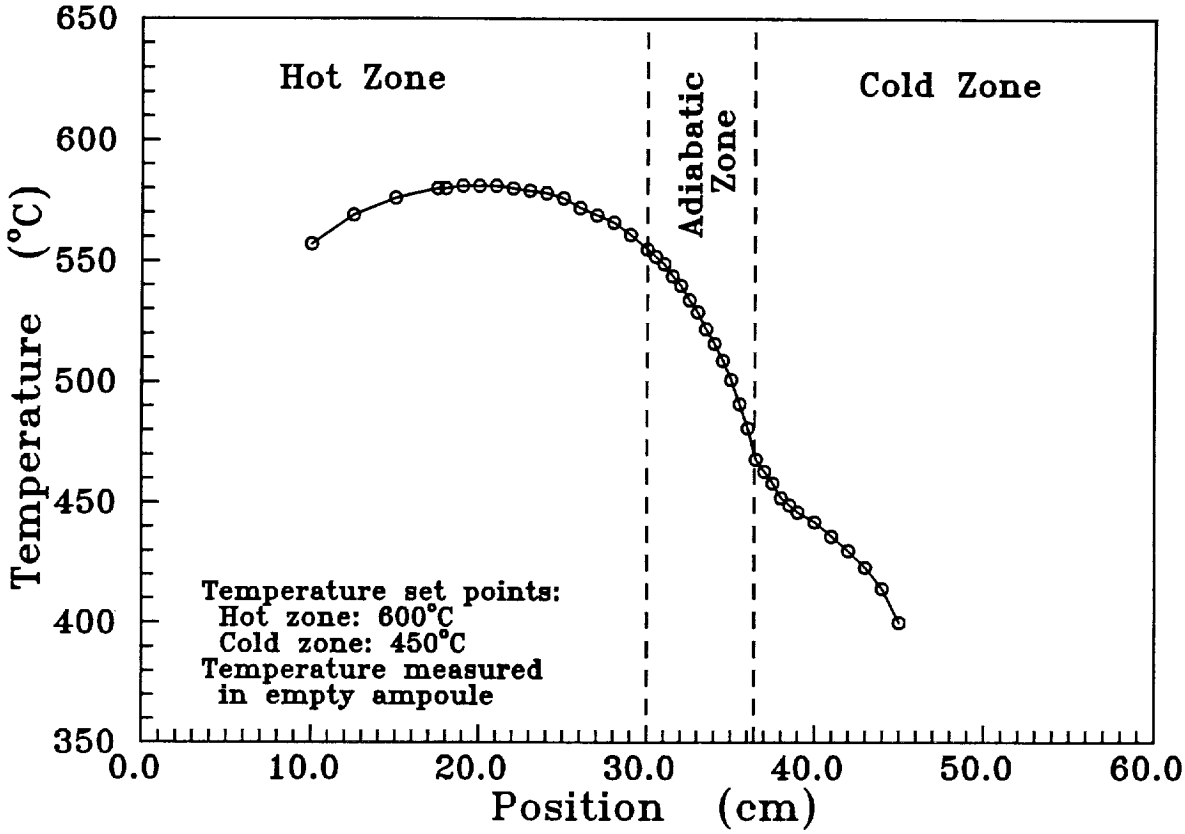

Figure 4 Quenched interface demarcation schedule

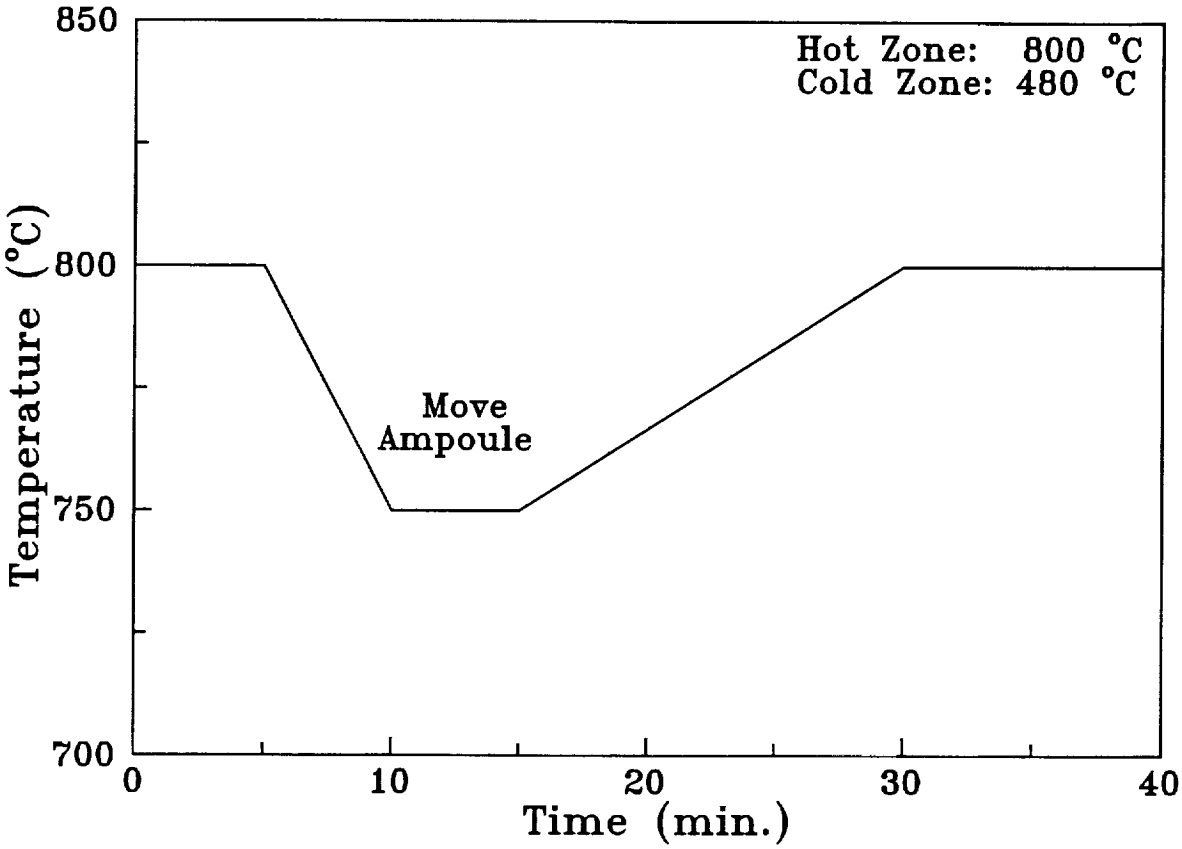

Figure 5 Ampoule design for temperature measurement experiments

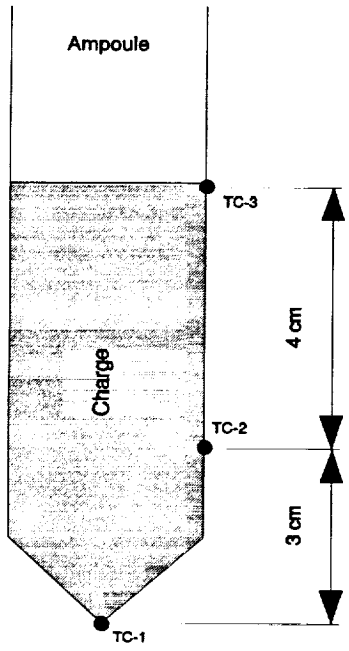

a. Ampoule for temperature profiles measurement

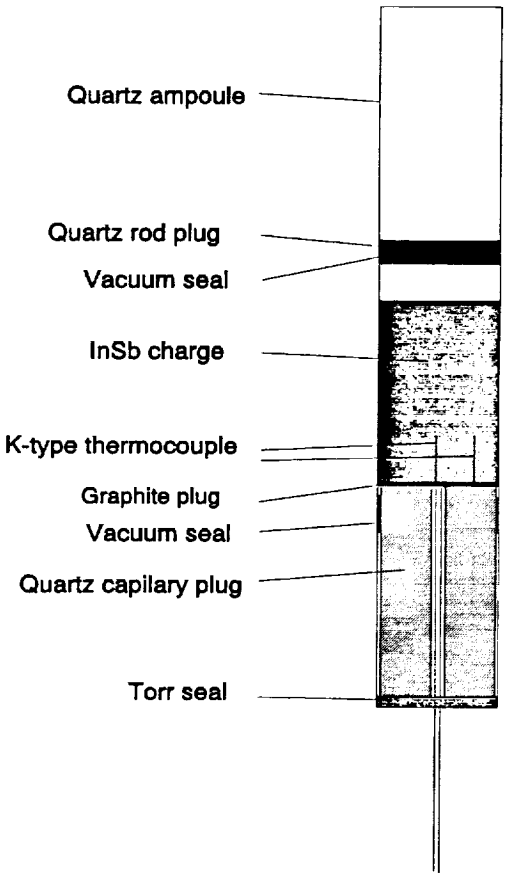

b. Ampoule for temperature in melt measurement

Figure 6 Axial composition profiles for InSb-GaSb ingots

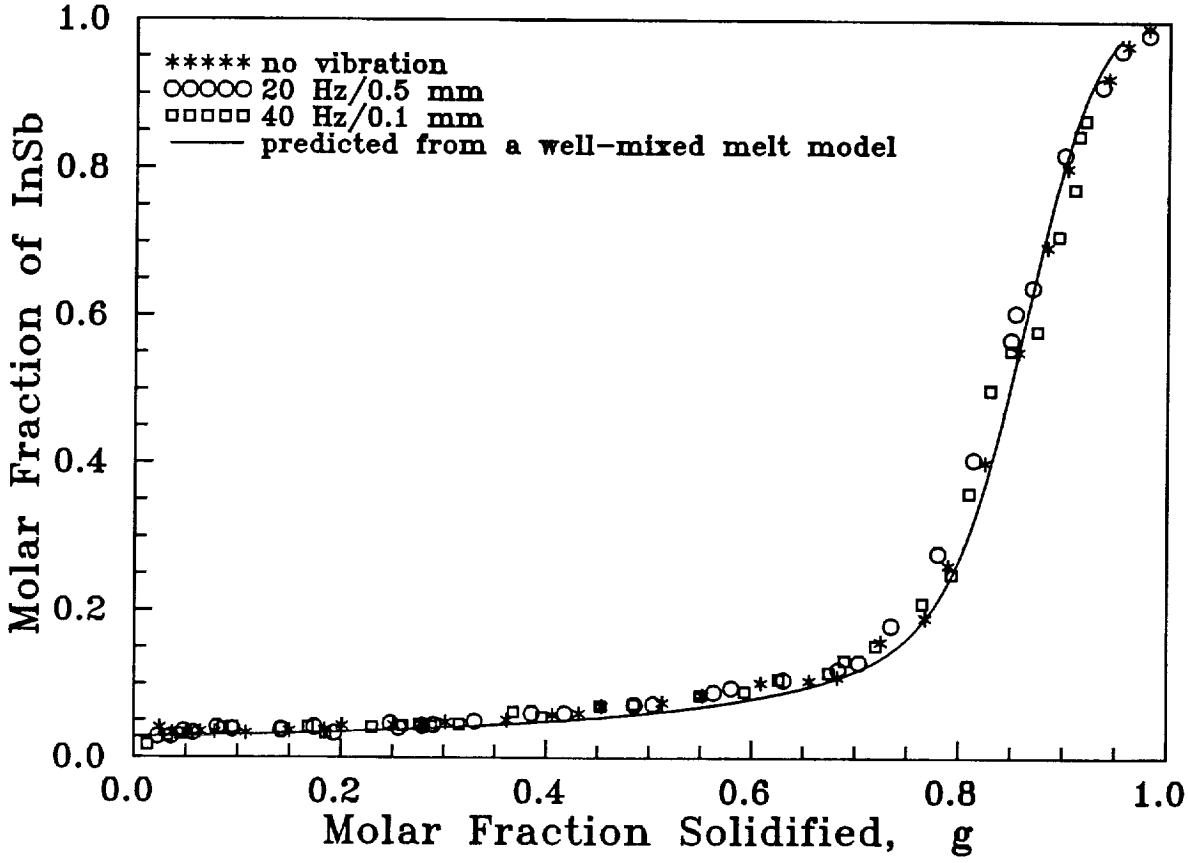

Figure 7 Radial compositional profiles for InSb-GaSb ingots

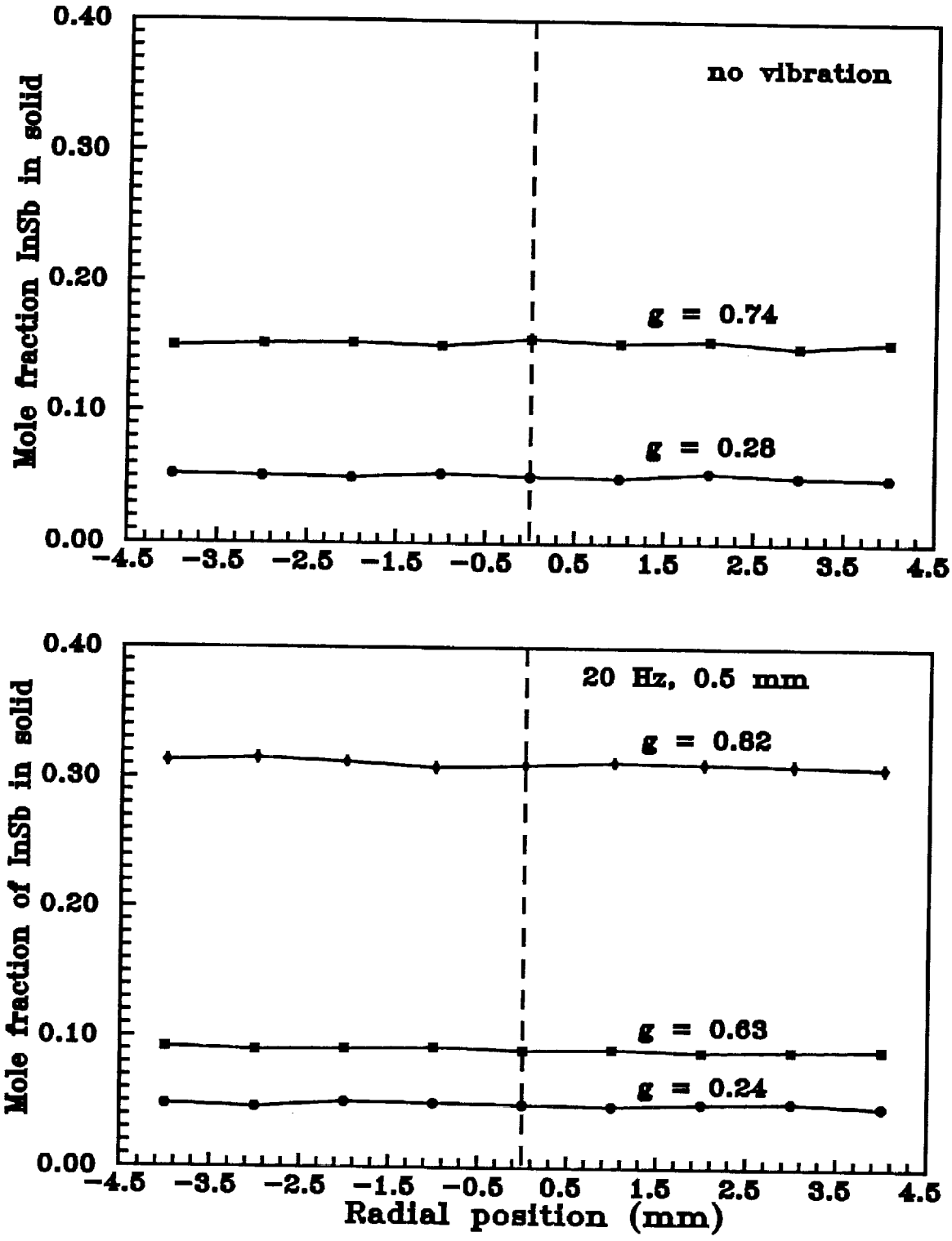

Figure 8 The average growth rate for solidification of InSb-GaSb

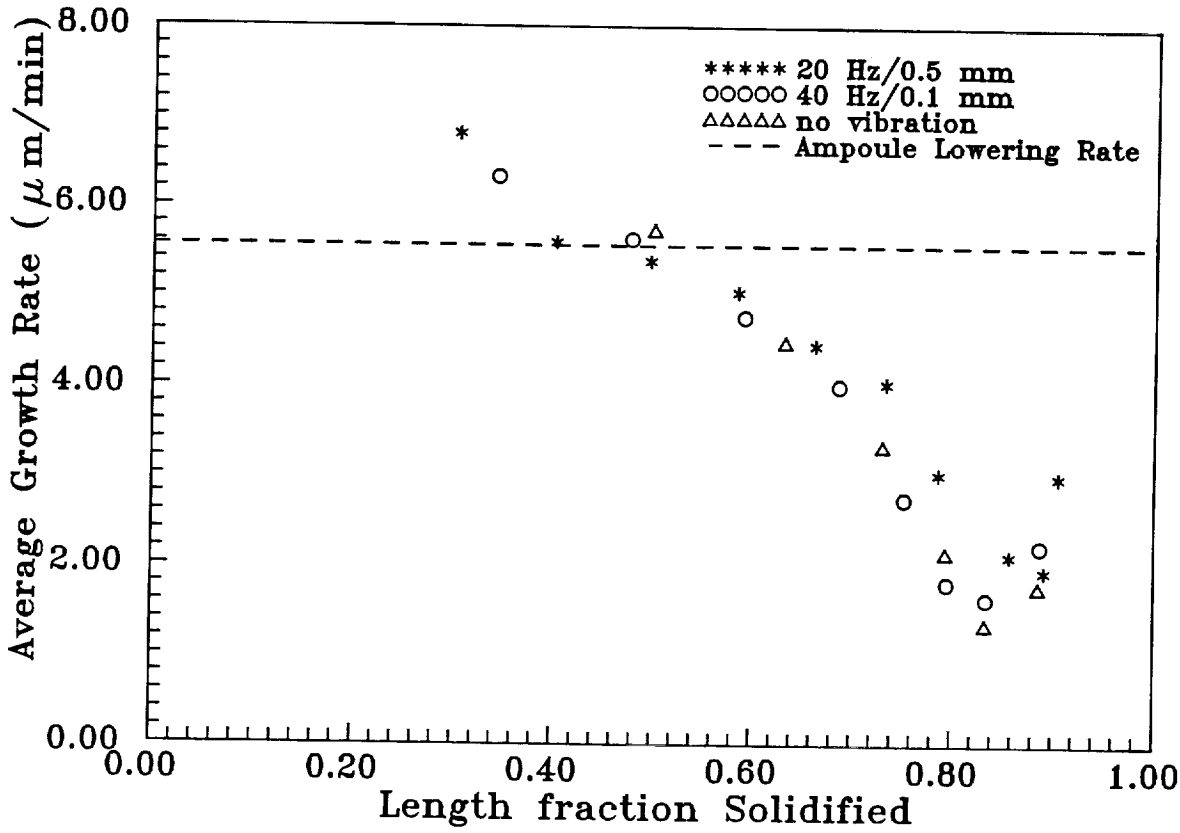

Figure 9 Interface depth for solidification of InSb-GaSb

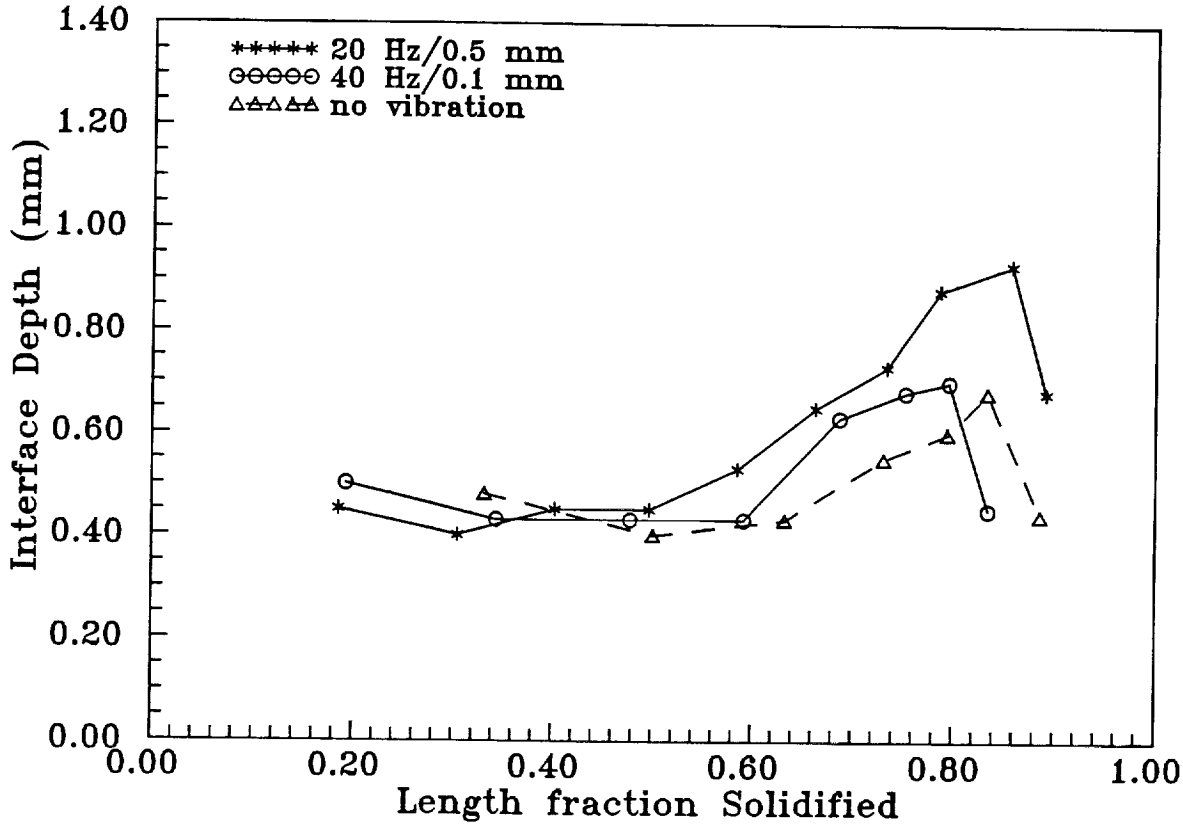

Figure 10 The relative interface velocity for solidification of InSb-GaSb

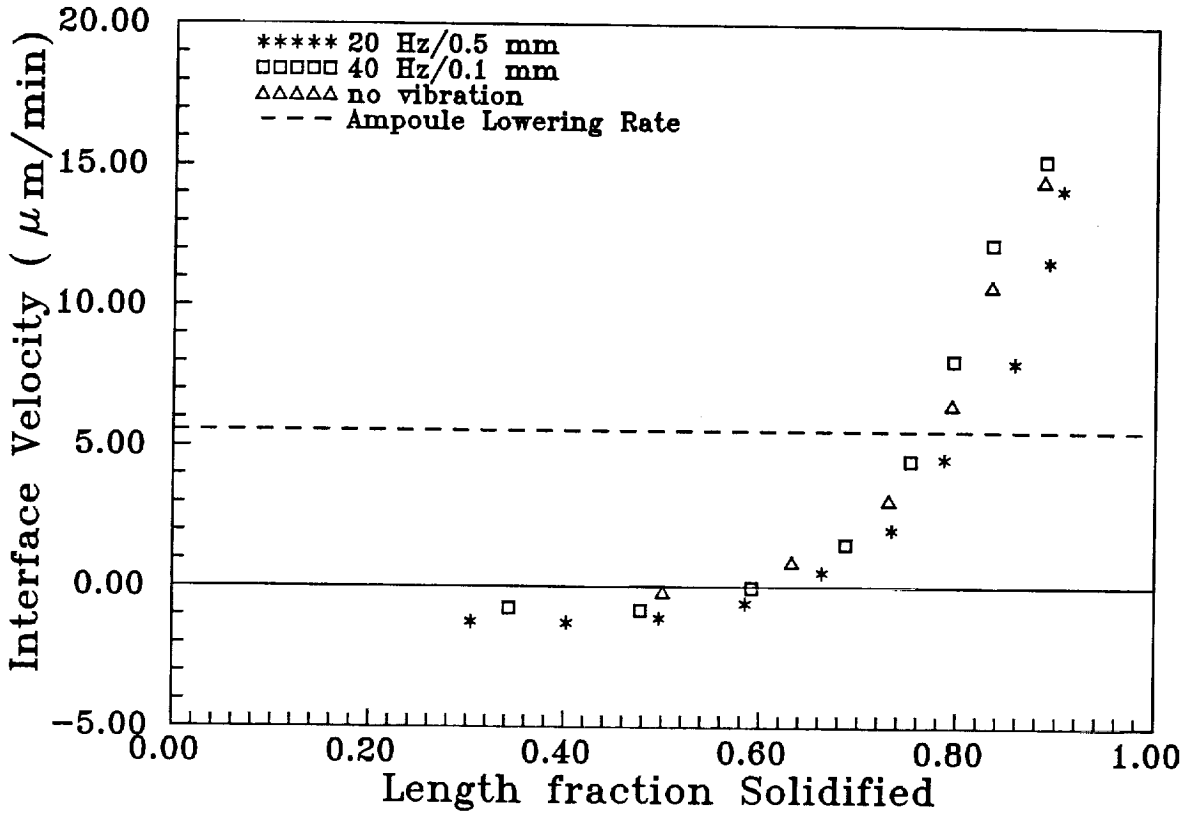

Figure 11 Photography shown the microstructure of InSb-GaSb ingots
left: no vibration, right: 20 Hz/0.5 mm amplitude vibration

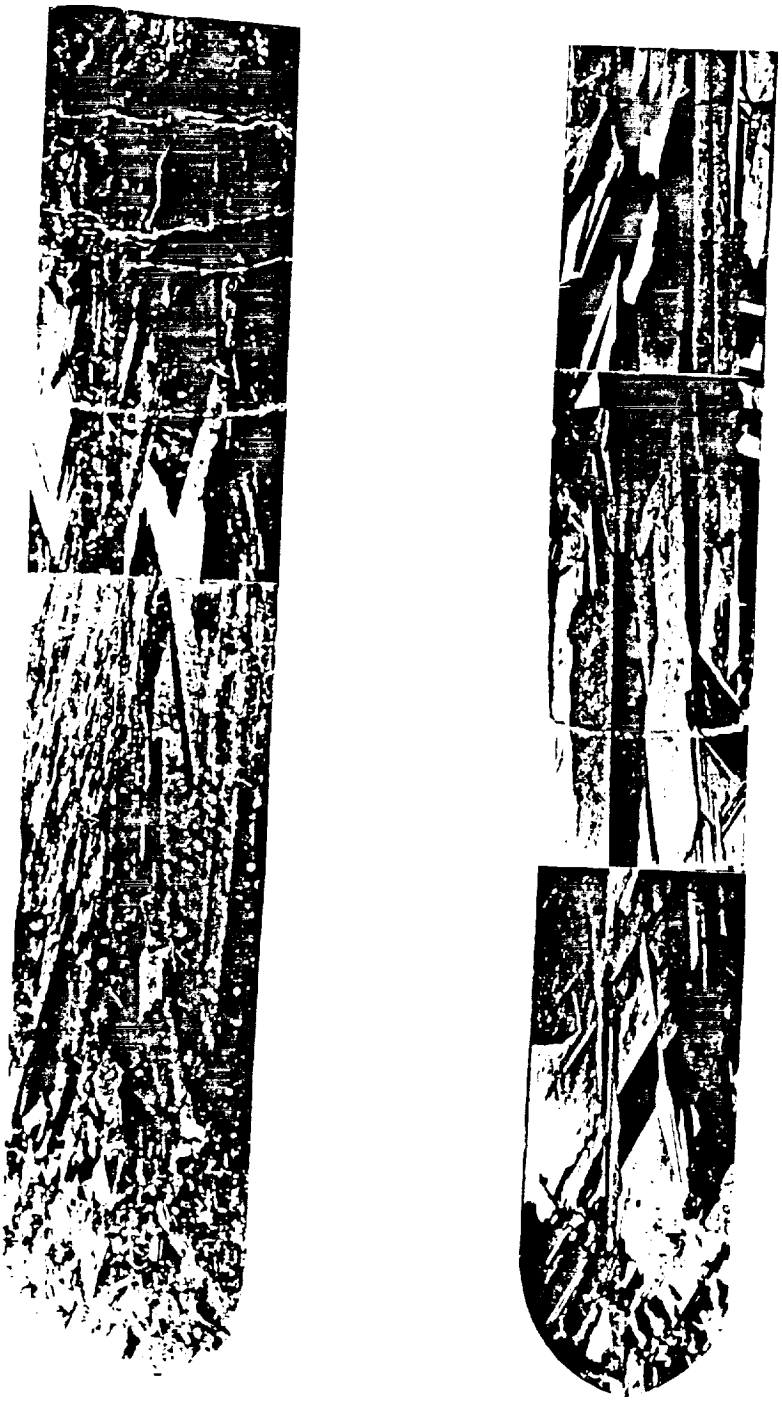

Figure 12 Number of boundaries for InSb-GaSb ingots

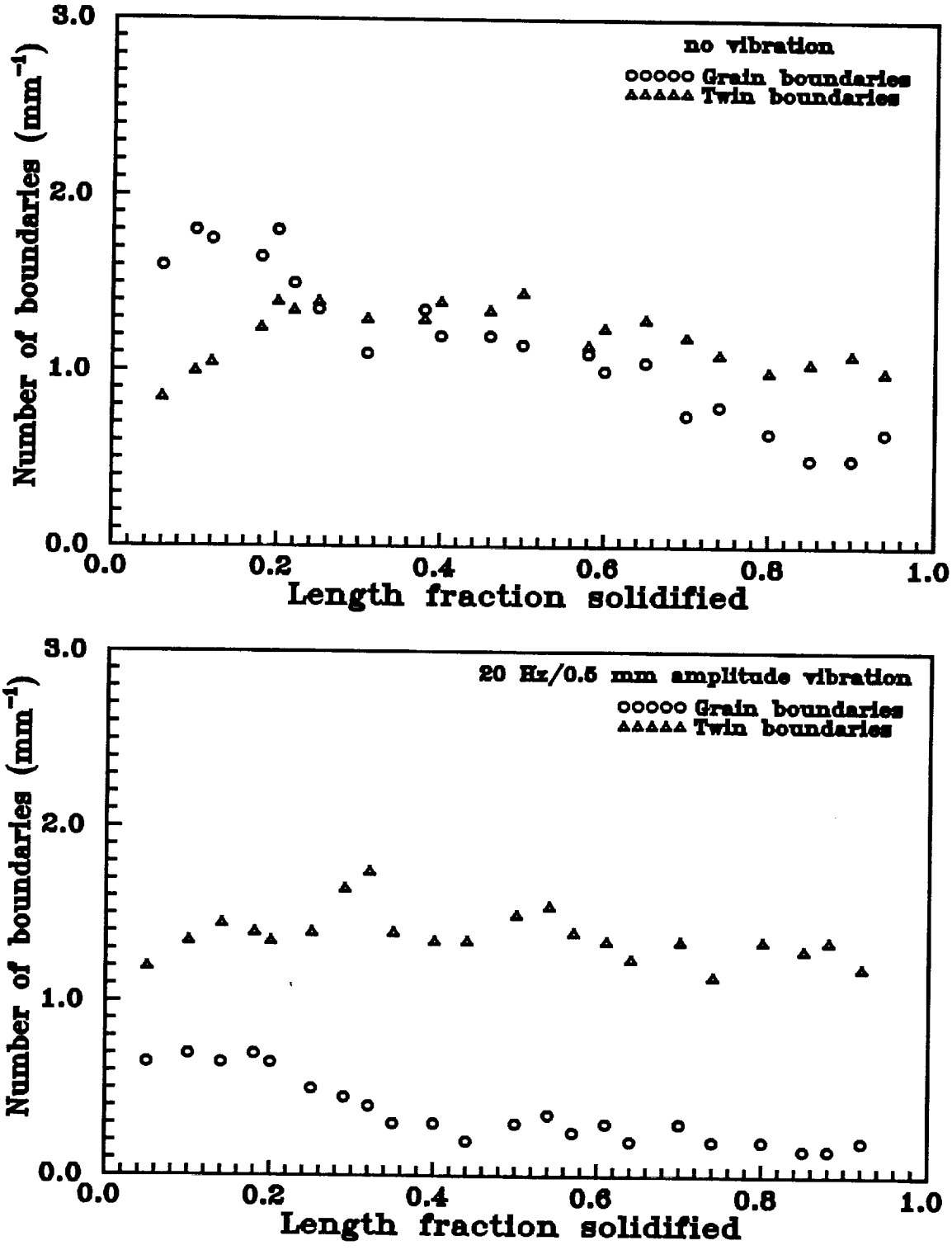

Figure 13 The effect of dynamic acceleration on the number of boundaries of InSb-GaSb ingots

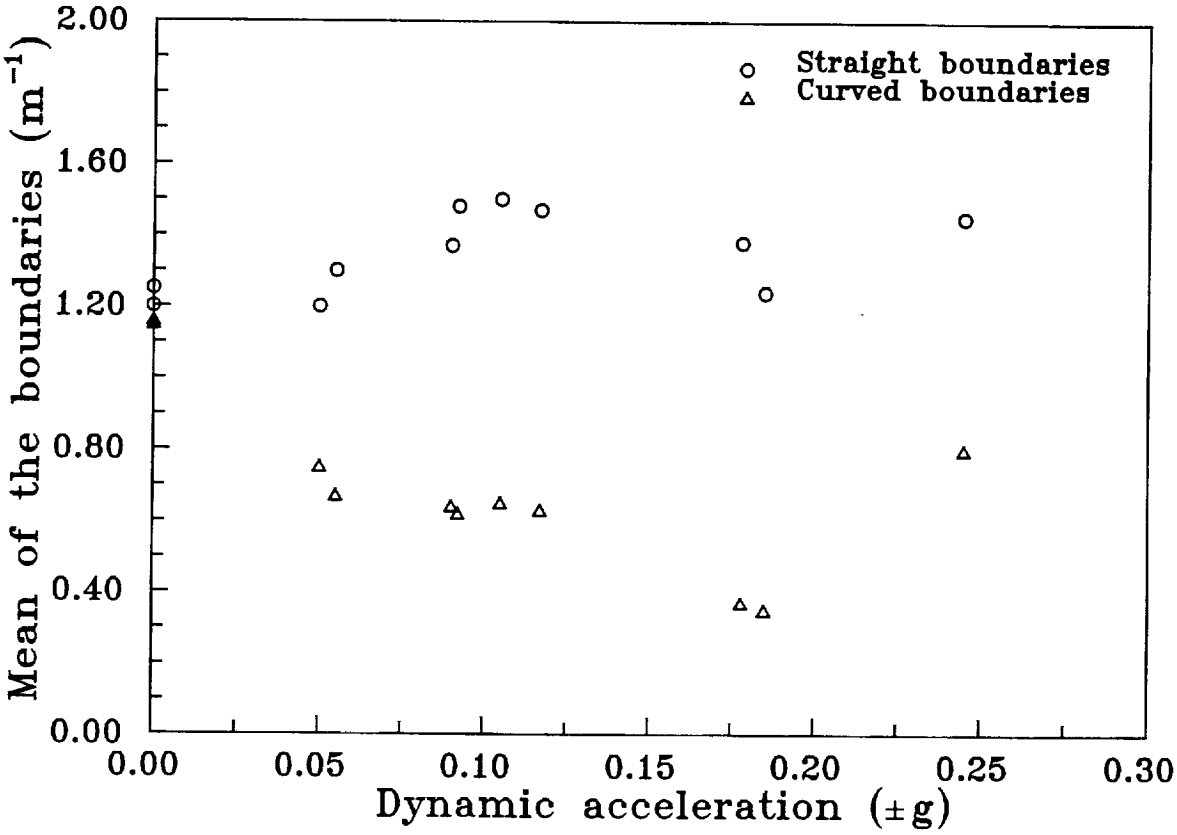

Figure 14 Growth rate for solidification of InSb

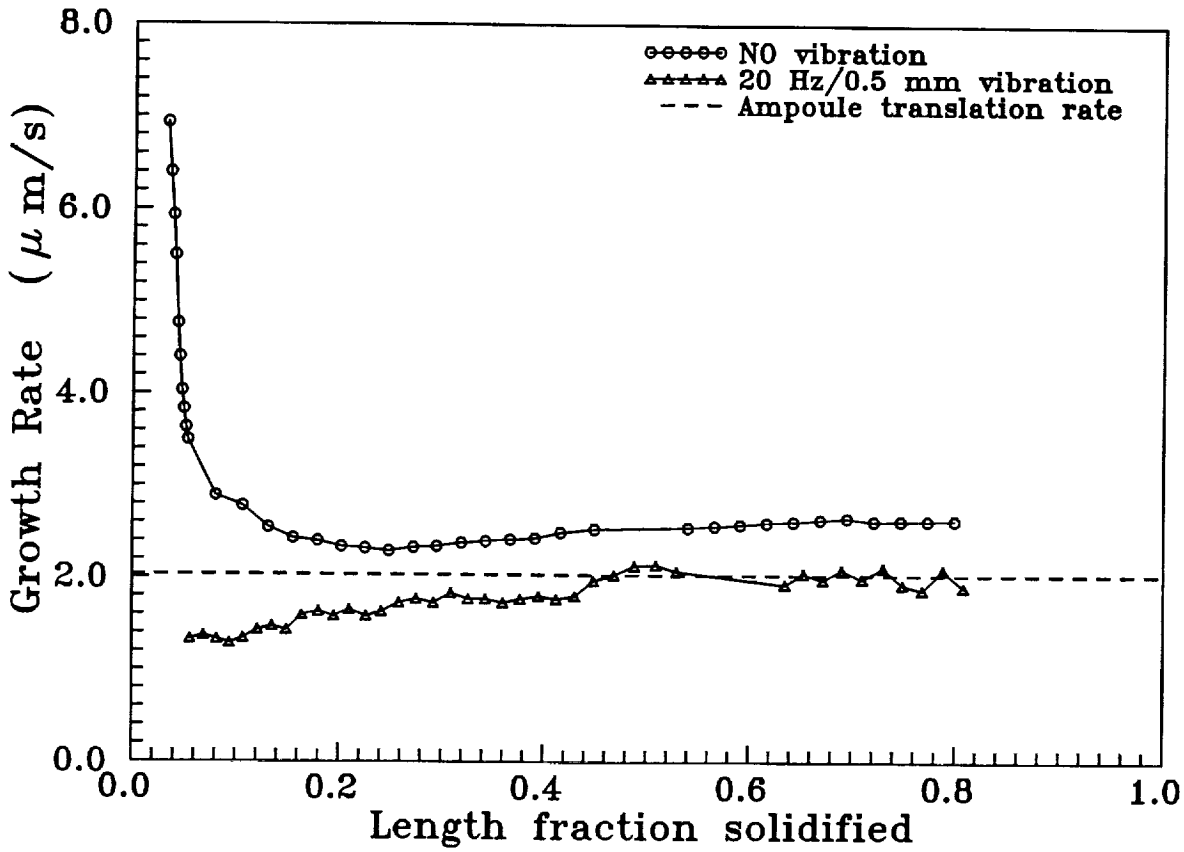

Figure 15 Photography shown the microstructure of InSb ingots
upper: no vibration, lower: 20 Hz/0.5 mm amplitude vibration

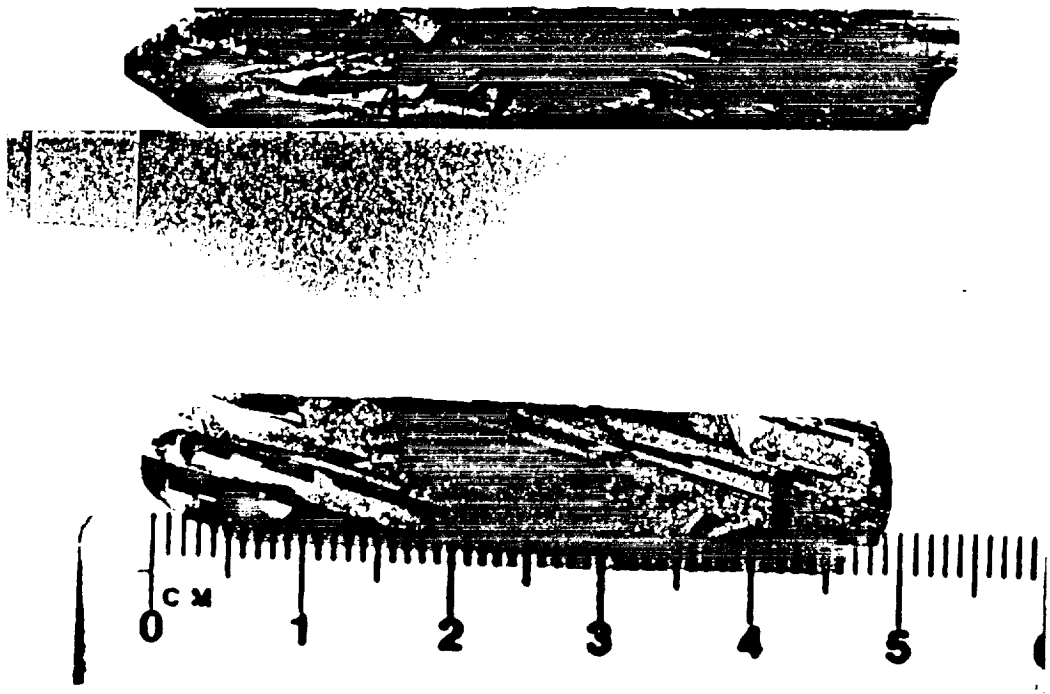

Figure 16 Photography shown the microstructure of InSb ingots
a. no vibration, b. 20 Hz/0.5 mm amplitude vibration, 1 min. on/5 min. off
c. 20 Hz/0.5 mm amplitude vibration, 5 min. on/1 min. off

Figure 17 Photography shown the microstructure of 22 mm diameter InSb ingots upper: no vibration, lower: 20 Hz/0.5 mm amplitude vibration

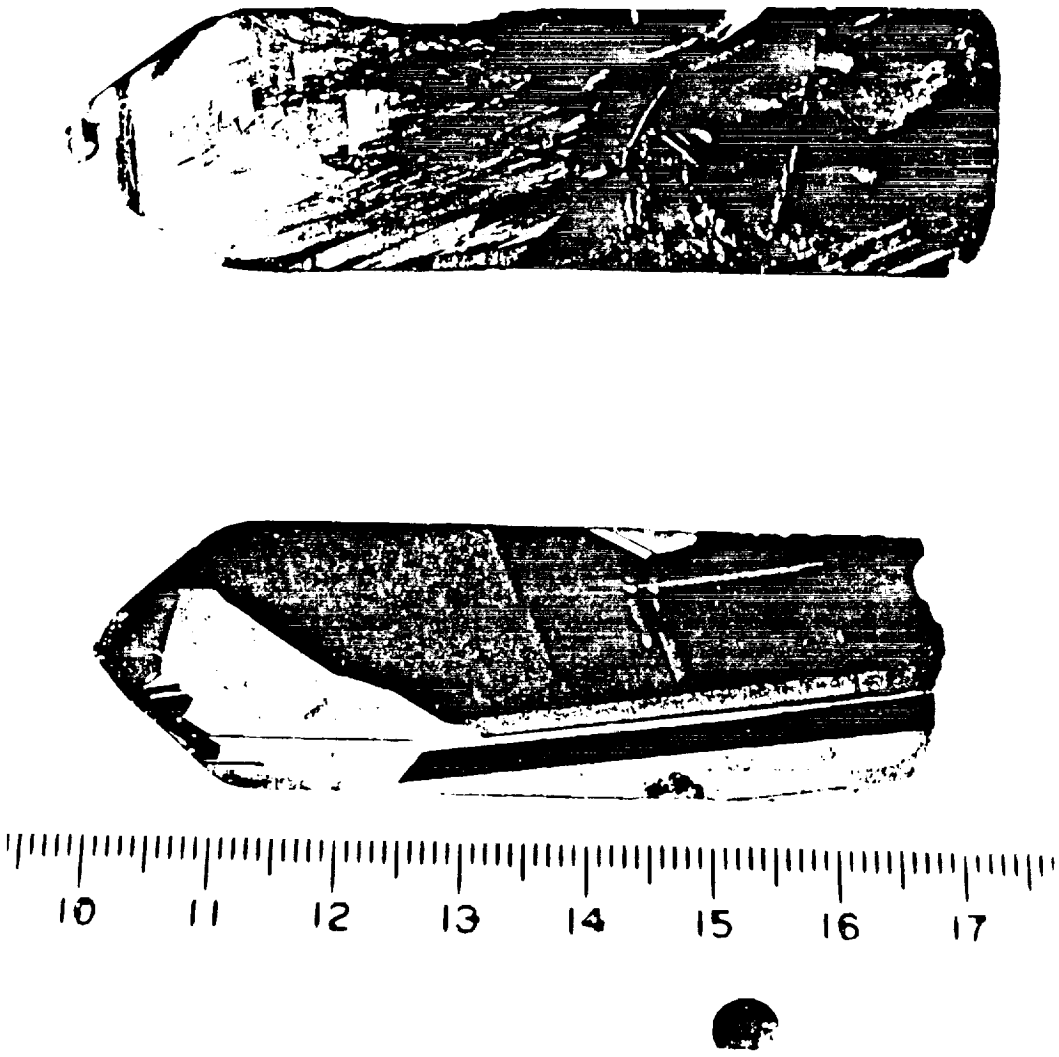

Figure 18 Axial resistivity profiles for InSb ingots

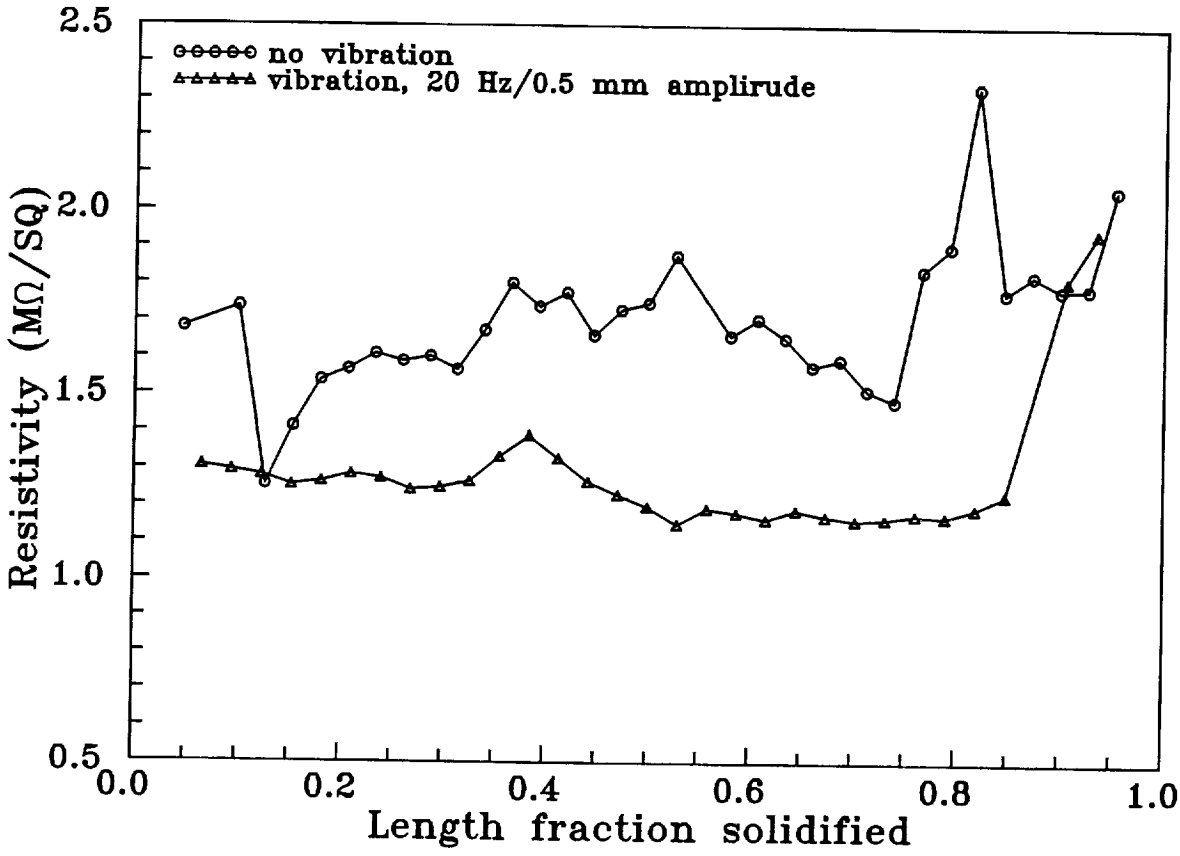

Figure 19 Radial resistivity profiles of InSb ingots

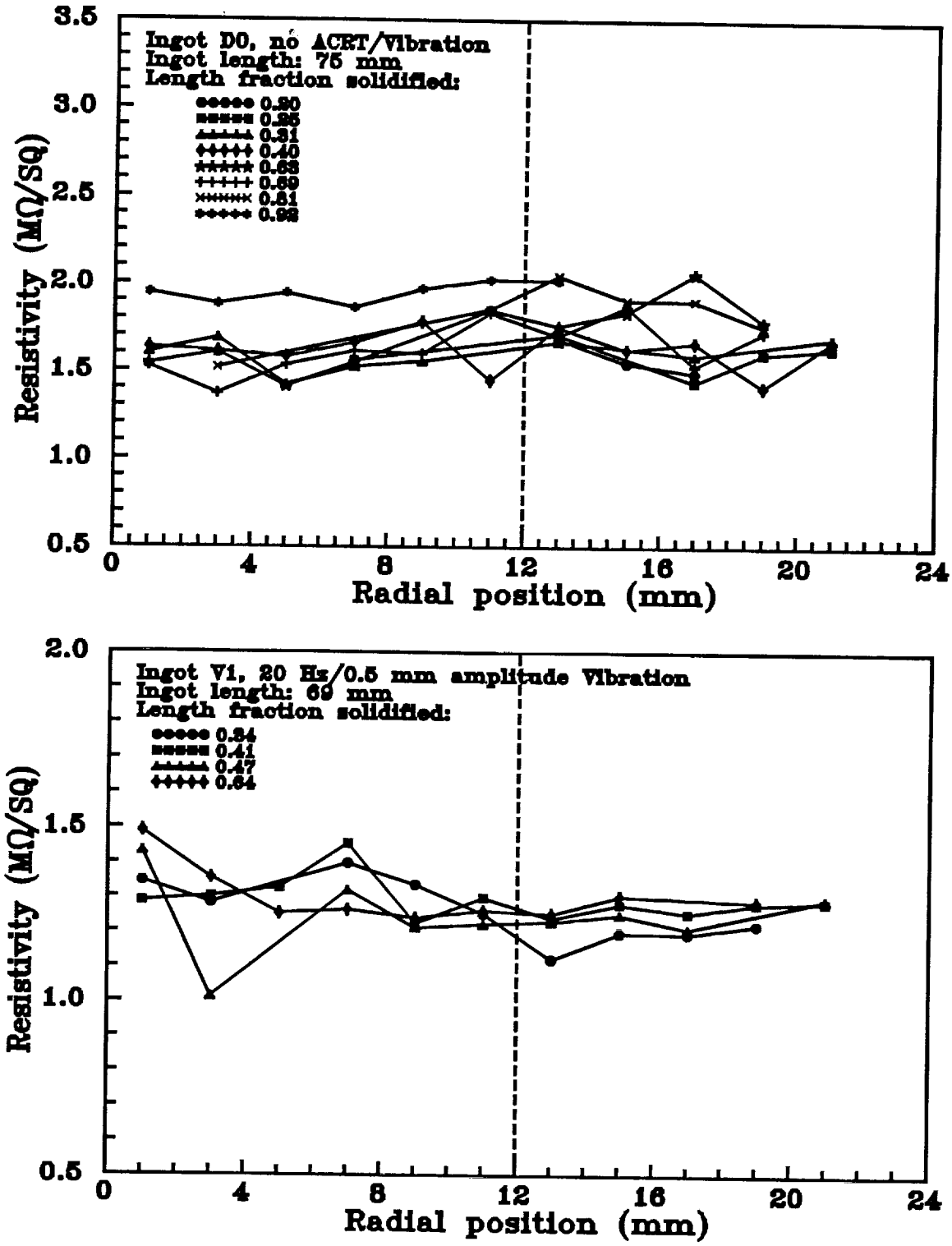

Figure 20 Photography shown the microstructure of InSb ingots
upper: no ACRT, lower: 80 rpm ACRT, 20 aec. on/20 sec. off

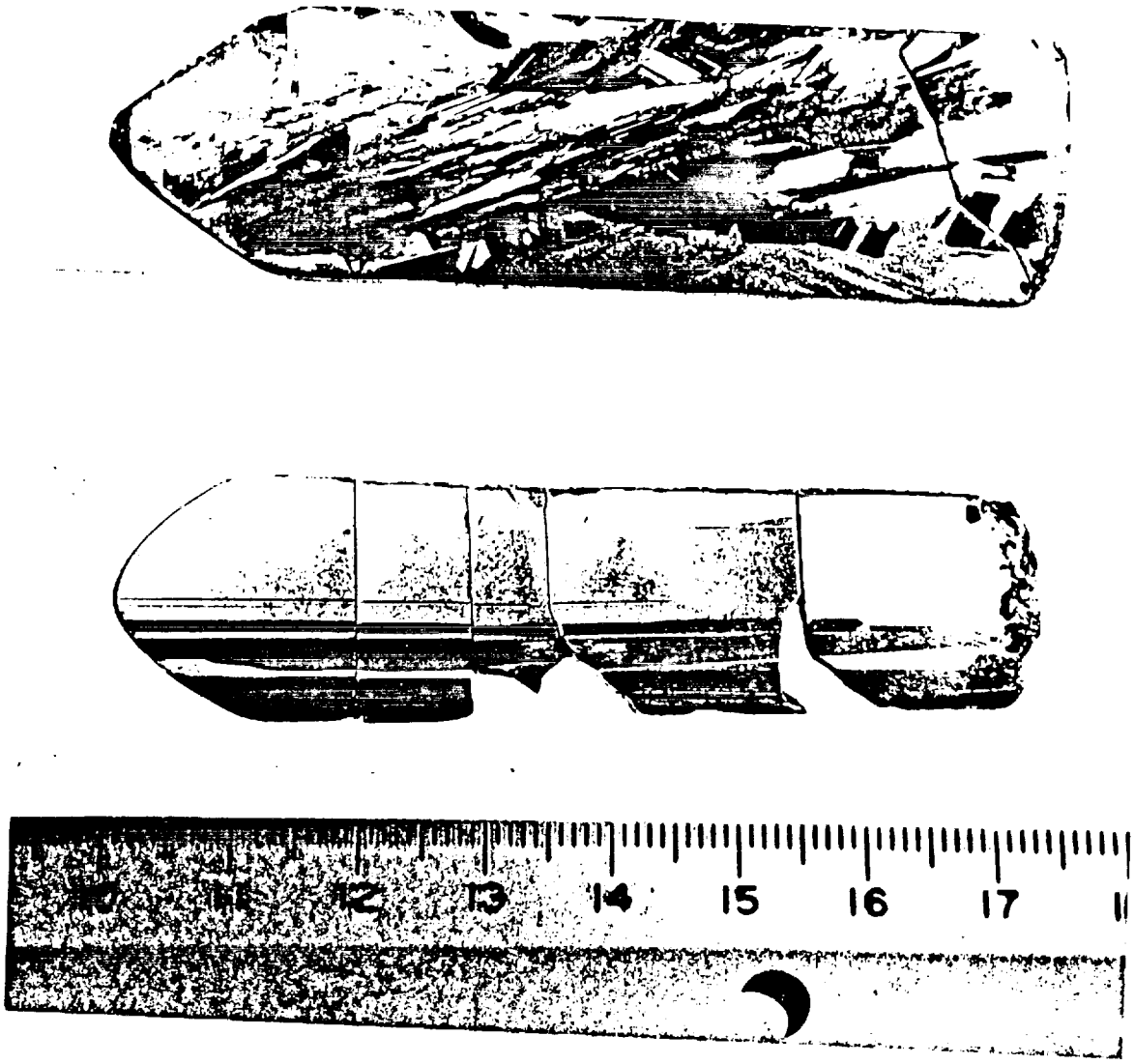

Figure 21 Temperature profiles measured at bottom center of the ampoule

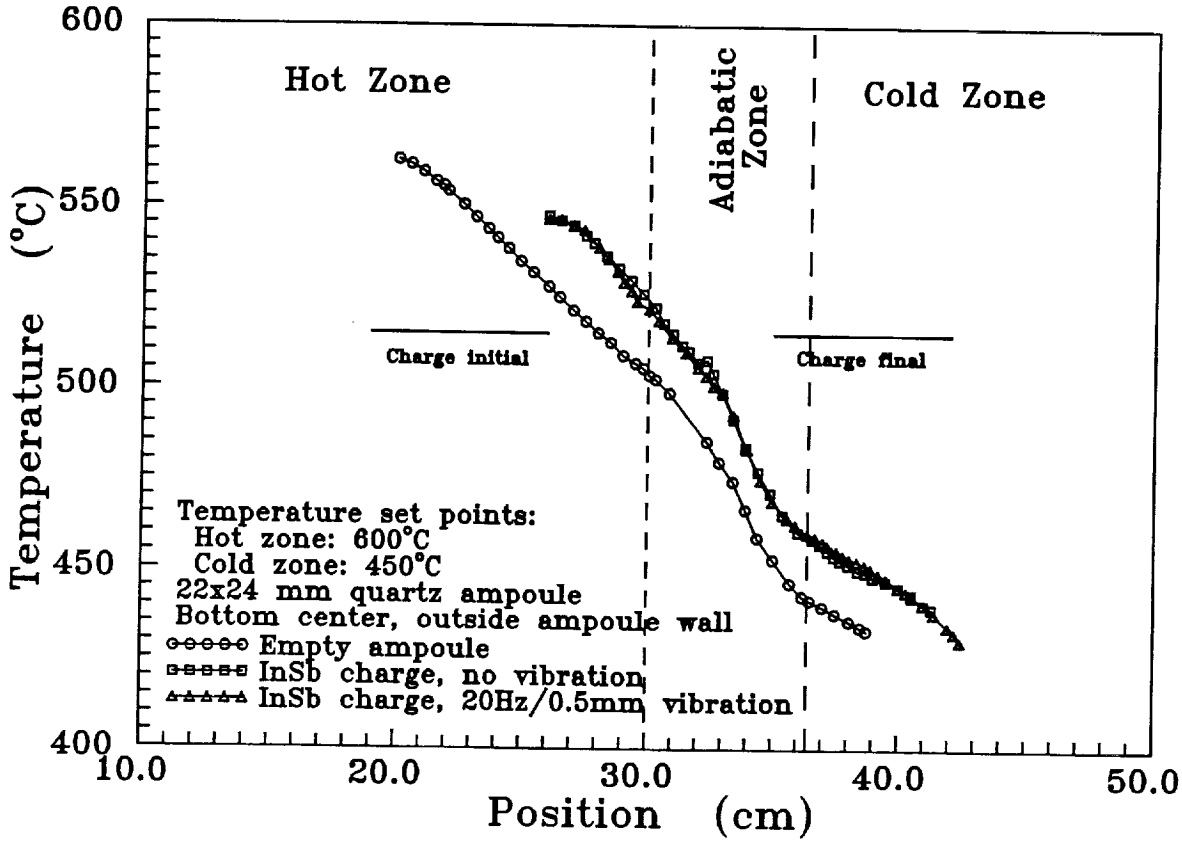

Figure 22 Temperature profiles measured at 3 cm above bottom center of the ampoule

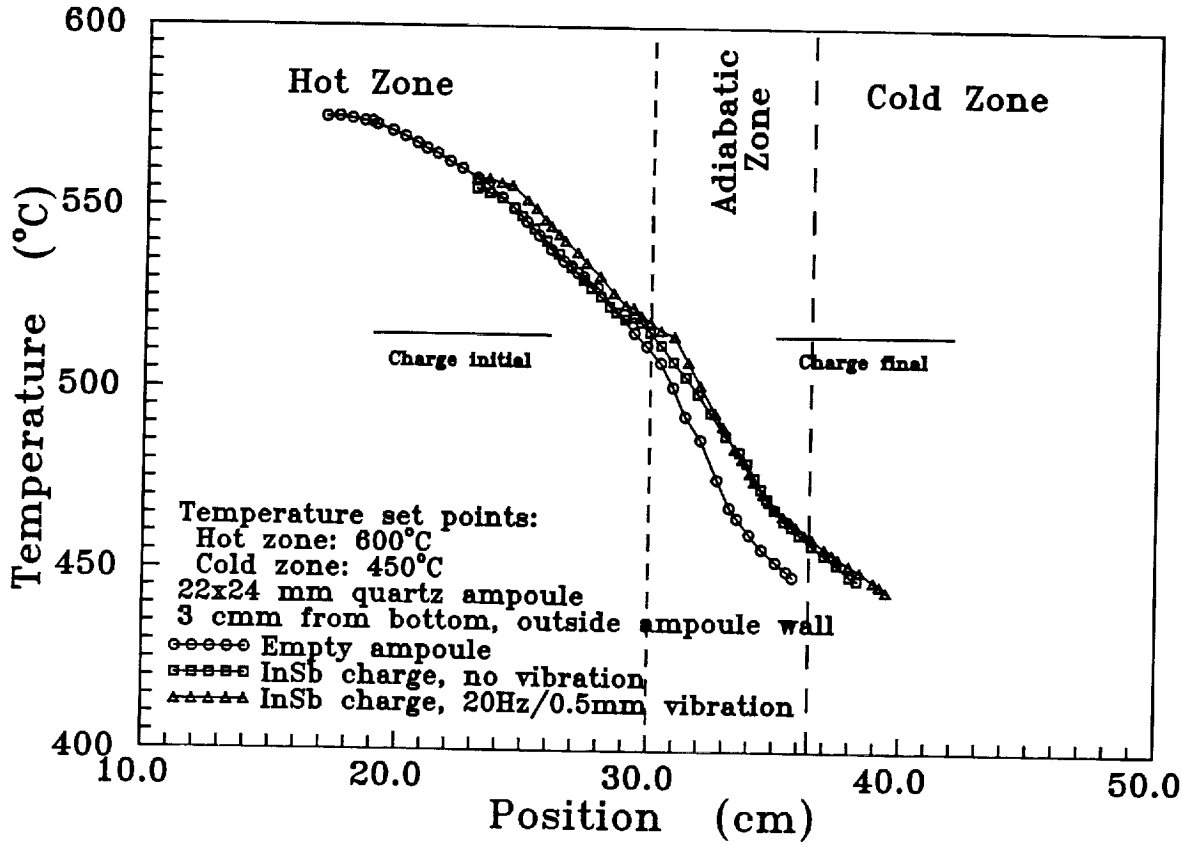

Figure 23 Temperature profiles measured at the top of the charge

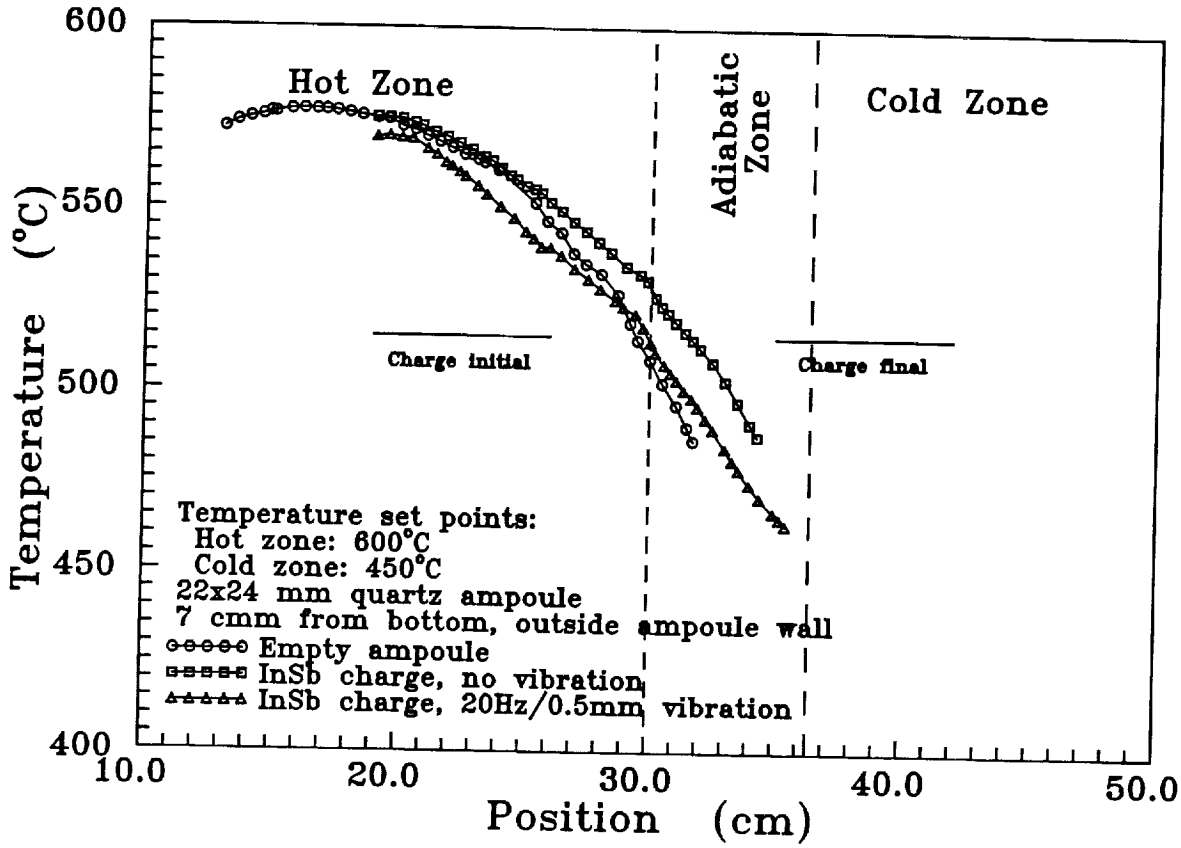

Figure 24 Temperature in the melt far away from the solid/melt interface

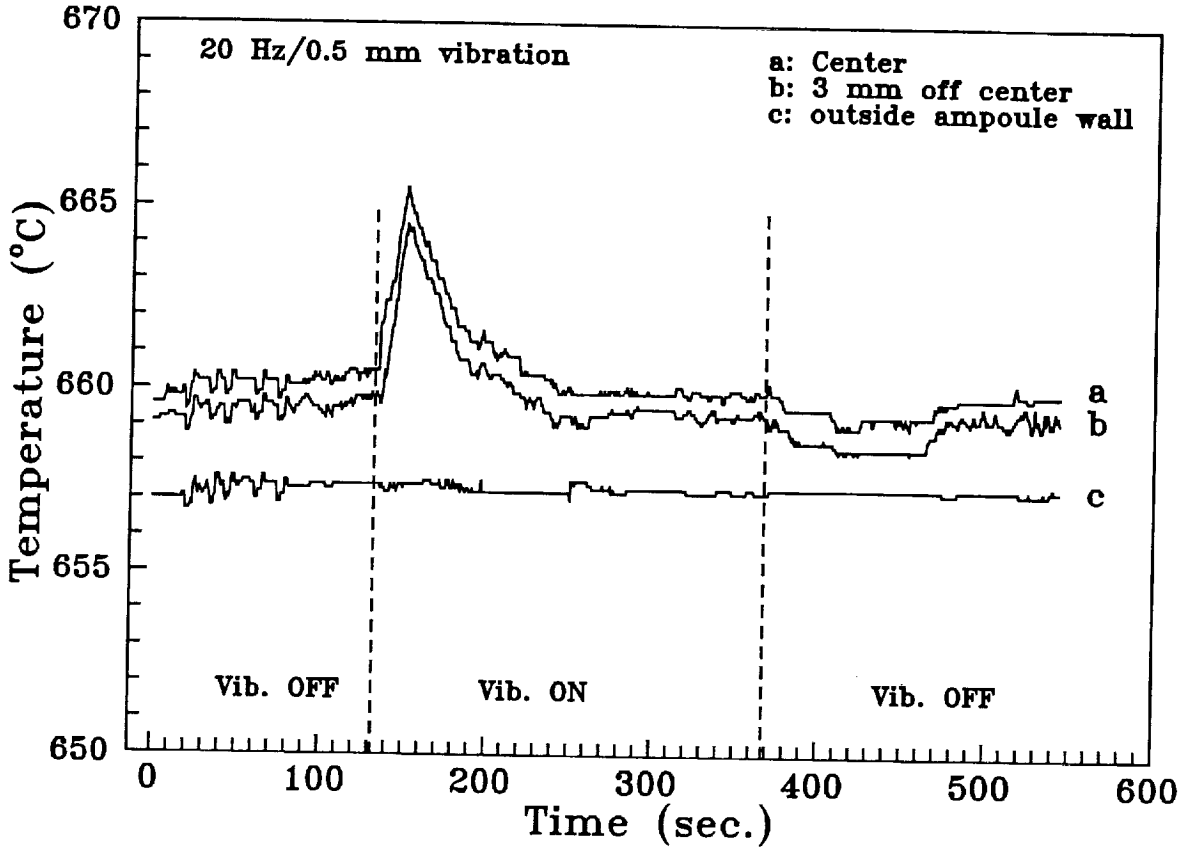

Figure 25 Temperature in the melt near the soli/melt interface

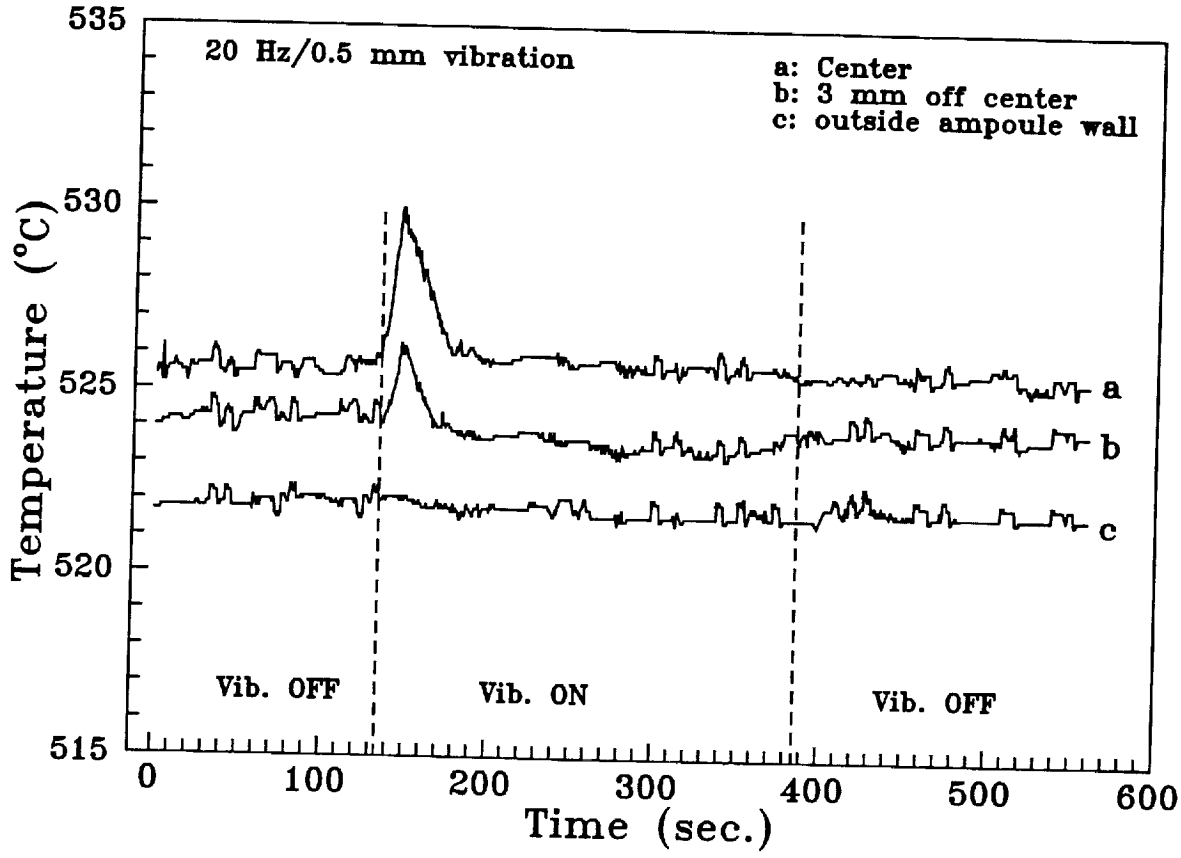

Figure 26 Heat translation coefficient between the charge and the furnace

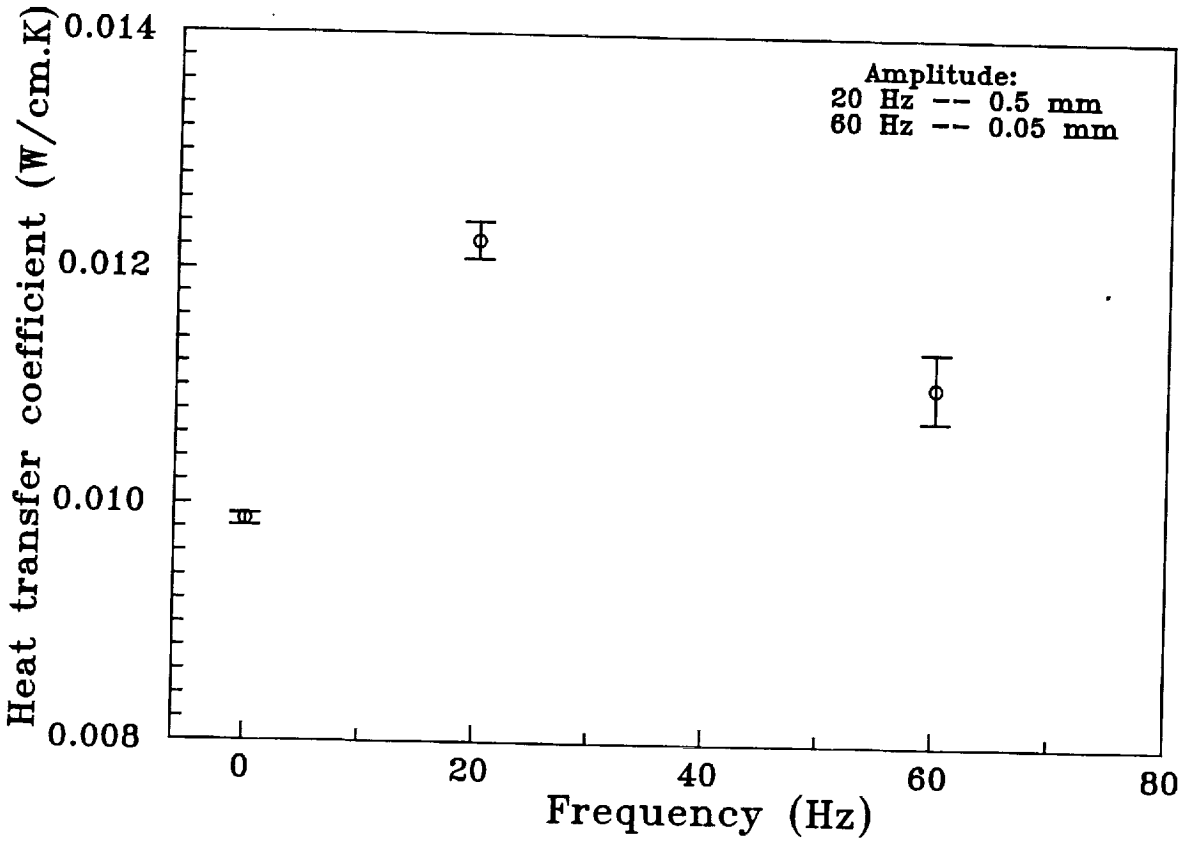

Figure 27 Axial resistivity profiles for InSb ingots

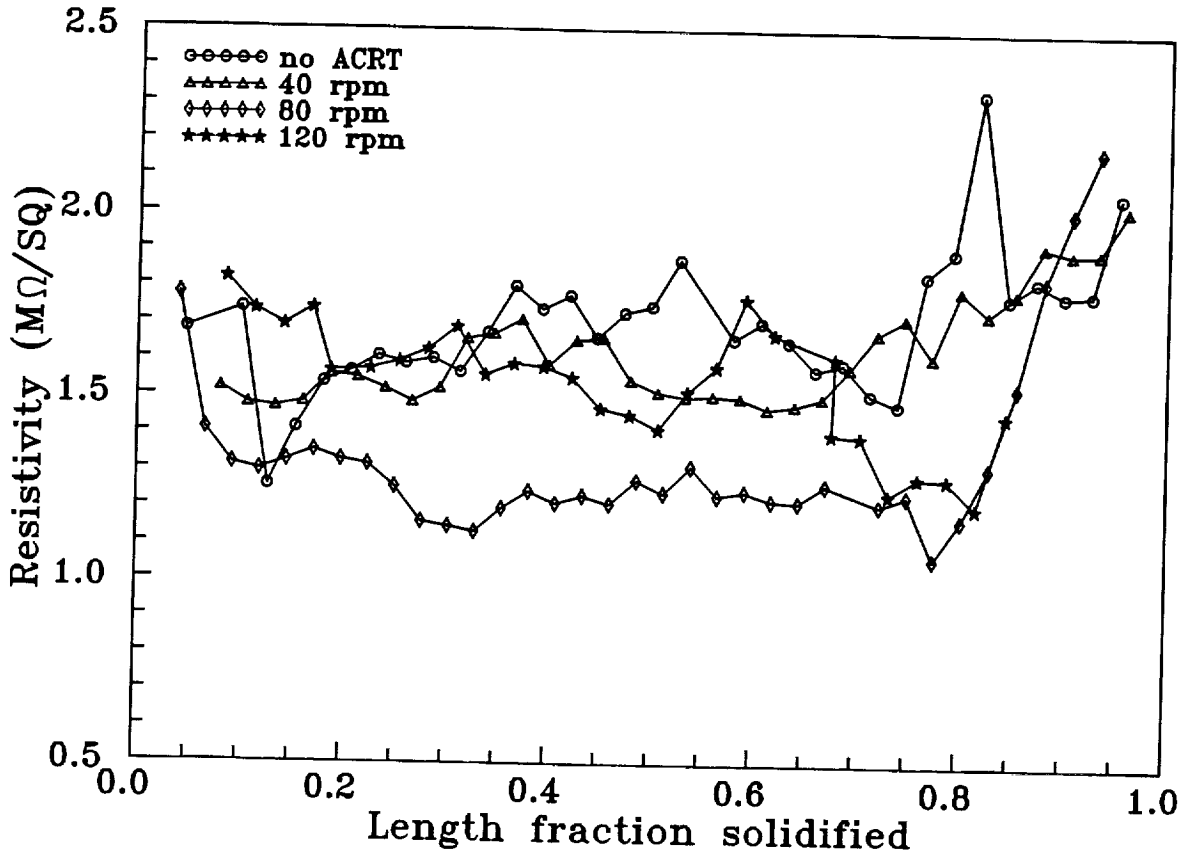

Figure 28 Radial resistivity profiles for InSb ingots